



# Corrosion Fatigue & Life Optimalisation of offshore wind turbine monopiles

Summary report of the C-FLO project

Henk Slot (TNO)
Stefan Jansen (Deltares)
Bert Sluys (TU Delft)
Erik Schuring (TNO)
Richard Pijpers (TNO)
Jorrit Rodenburg (TNO)
Joke Luyten (TNO)

28 October 2023





# **Table of contents**

1	Intr	oduction	4
2	Corı	osion protection of monopile	6
	2.1	Introduction	6
	2.2	Corrosion protection scenarios	6
3	Det	erministic Pit corrosion – fatigue model – WP2	. 11
	3.1	Introduction	. 11
	3.2	Model description	. 11
	3.3	Model for the Pit-to-Crack Transition	. 12
	3.4	Propagation module	. 14
	3.5	Input parameters	. 15
	3.6	Conclusion	. 17
4	Fun	damental pit corrosion & mechanical loading model – WP2	. 17
	4.1	Introduction	. 17
	4.2	Corrosion pit growth & mechanical loading modelling	. 17
	4.3	Conclusion	. 20
5	Ехр	erimental results - WP3	. 20
	5.1	Introduction	. 20
	5.2	Pit corrosion – exposure of coupons in offshore monopiles	. 21
	5.3	Exposure & measurements in microbiologically enriched seawater	. 23
	5.4	Exposure of coupons in artificial seawater (without MIC)	. 24
	5.5	Pitting-corrosion data obtained from literature, as for welded joints	. 25
	5.6	Summary of corrosion rates for various zones	. 25
	5.7	Corrosion-fatigue test results	. 26
6	Cori	osion-fatigue tests on dogbone coupons at Vattenfall	. 28
	6.1	Introduction	. 28
	6.2	Test set up	. 28
	6.3	Pre-corrosion of specimens	. 30
	6.4	Corrosion – fatigue test results	. 32
	6.5	Conclusion	. 33
7	Mod	del results – S-N curves - WP4	. 33
	7.1	Introduction	. 33
	7.2	Cathodic protection in seawater environment	. 34
	7.3	Free corrosion environment	. 35
	7.4	Modelling results – S-N curves	. 35







	7.5	Sensitivity analysis	. 41
	7.6	Conclusions	. 43
8	Mor	nopile design - WP4	. 43
	8.1	Introduction	. 43
	8.2	Corrosion protection scenarios & Design matrix	. 44
	8.3	Case I - Design thickness - Only FLS criterion	. 44
	8.4	Case II - Design fatigue life - Only FLS criterion	. 45
9	Con	clusions & Recommendations	. 45
	9.1	Conclusions	. 45
	9.2	Recommendations	. 48
10	Refe	erences	. 49





## 1 Introduction

The project Corrosion Fatigue Life Optimisation (C-FLO) executed between 2019 and 2023 is part of the joint research program on offshore wind energy GROW [1]. The GROW program aims to reduce costs of offshore wind electricity, to create added value for the Dutch economy, and to strengthen the Dutch offshore wind industry. The project is supported by the Dutch Ministry of Economic Affairs and Climate Policy and TKI Offshore Energy (part of Energy InnovationNL).

# **Project partners**

The consortium comprises wind farm developers and owners, contractors, manufacturers, suppliers, authorities, and research organisations, see Table 1.

Table 1. Project partners

Consortium Partner	Company logo
TNO	TNO
Deltares	Deltares
TU Delft	<b>T</b> UDelft
Ørsted	Orsted
Eneco	Eneco
Van Oord	Van Oord  Marine ingenuity
Parkwind	PARKWIND
Sif	Sif
RWE	RWE
Shell	
Posco	boeco
PPG Coatings	PPG
DNV	DNV
Rijkswaterstaat	Rijkswaterszaat Ministerie von Verkeer en Waterstoot
Vattenfall	VATTENFALL 👄
GROW Office	<b>grow</b>





## **Objectives of the C-FLO project**

It is vital to properly evaluate the structural performance of offshore wind turbine monopiles and their foundations. The influence of environmental actions, such as corrosion by seawater and fatigue due to the cyclic mechanical loading, drive the amount of steel used in the structure, thus effective corrosion and fatigue mitigations measures are needed.

Throughout the various life stages of the monopile, multidisciplinary requirements result in suboptimal design and service life predictions. Hence, there is potential room for design improvements towards a lighter monopile as well as optimised corrosion protection methods. On the other hand, a too optimistic structural design might lead to unacceptable risks.

The objective of the C-FLO project is to *develop an advanced corrosion pit growth and fatigue crack initiation and growth model for the service life prediction of monopile foundations in the North Sea*.

The model aims at optimizing the monopile design and maintenance based on the improved understanding of the combined effect of corrosion and fatigue on the service life of monopile foundations. The optimised design of the monopile and corrosion protection systems lead to a reduced CAPEX in material use and installation, and optimised maintenance strategies brings down the OPEX. In addition, the model enables quantification of effects on the service life due to the temporary absence of cathodic protection.

Figure 1.1 presents a schematic overview of the content of the WP1, 2, 3 and 4.

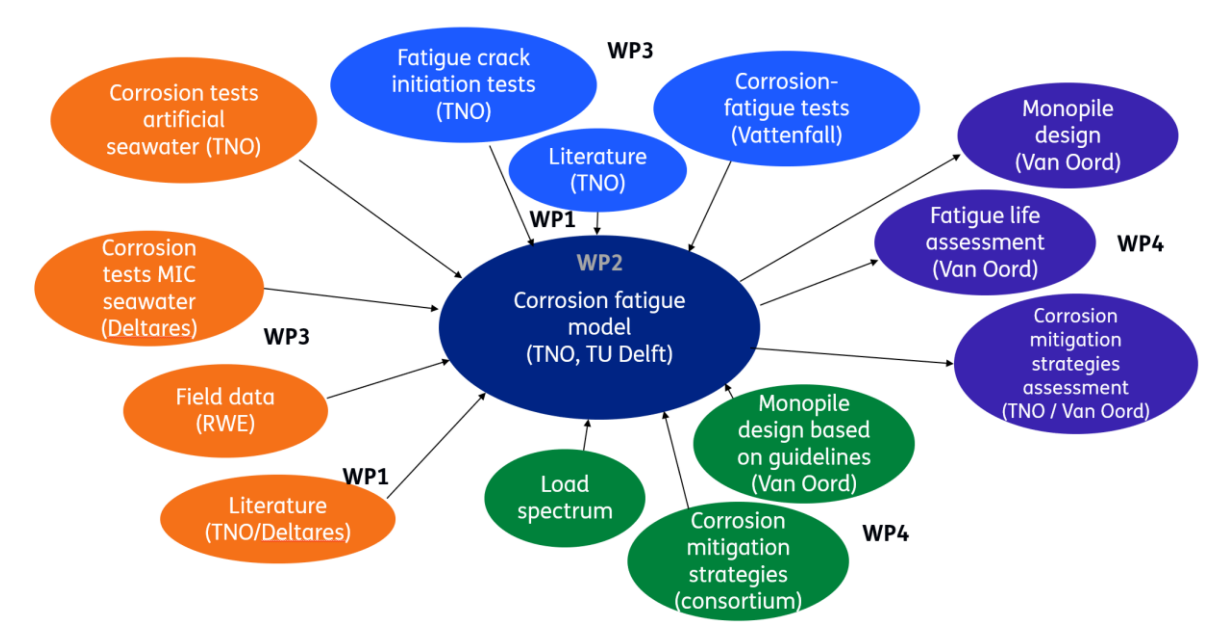


Figure 1.1 - Schematic Overview Work Packages.

The industrial partners, Van Oord Offshore Wind has directly used (WP4) model prediction results for an updated design of a reference (example case) monopile and the corrosion-fatigue model has been used to calculate remaining structural life accounting for various design and corrosion protection strategies.





In this report the following C-FLO project subjects have been summarized:

- Corrosion protection of monopile systems (WP1) in Chapter 2,
- Pit corrosion fatigue model (WP2) in Chapter 3,
- Pit corrosion & mechanical loading model (WP2) in Chapter 4,
- Experimental results (WP3) in Chapter 5 & 6,
- Model prediction results, S-N curves (WP4) in Chapter 7,
- Monopile design, performed by Van Oord Offshore Wind (WP4) in Chapter 8,
- General conclusions and recommendations in Chapter 9.

# 2 Corrosion protection of monopile

#### 2.1 Introduction

As a starting point of the C-FLO project, a reference monopile design has been selected. The focus was on the existing knowledge on corrosion and fatigue of critical locations in monopile foundations, including the effects of mitigation measures, see Table 2.1. Current practices in detailed design choices (such as weld quality) and corrosion mitigation have been brought in by the industrial partners.

Table 2.1 - Focus areas for reference details in a monopile foundation (welds, holes, materials, corrosion allowance).

Critical zones in the monopile	Corrosion mitigation		
<ul> <li>Outside, splash zone</li> <li>Inside, water column</li> <li>Inside, mudline</li> <li>Boat landing</li> </ul>	<ul> <li>Cathodic protection (GACP, ICCP),</li> <li>Protective coating, surface treatment</li> <li>Corrosion allowance by increased wall thickness and or steel type choice</li> </ul>		

Typical environmental conditions representing the Dutch North Sea have been evaluated based on available data from field tests from RWE and Parkwind.

The representative structural actions (external mechanical loadings) for a representative offshore wind turbine have been provided by Van Oord Offshore Wind [2], [3].

#### 2.2 Corrosion protection scenarios

In this section, the selected corrosion scenarios are described that formed the basis for further evaluation. In this C-FLO study five zones (external & internal) of the monopile structure have been considered, see Figure 2.1:

- · Atmospheric zone,
- Splash zone,
- Submerged zone,
- Top buried zone,
- Buried zone.

Figure 2.1a gives an overview of the 9-10 MW wind turbine considered in this study. The monopile is from -63 m below the lowest astronomical tide (LAT) to 20 m above the LAT. The water depth is -35 m LAT. The monopile is divided into different zones (i.e. elevation levels) to accommodate for different corrosion rates. Figure 2.1b presents these different zones in the monopile.





Measures to protect against corrosion are the use of coatings or cathodic protection. Measures for corrosion control:

- · Corrosion allowance,
- Cathodic protection (CP),
- · Coating systems,
- Use of corrosion resistant materials.

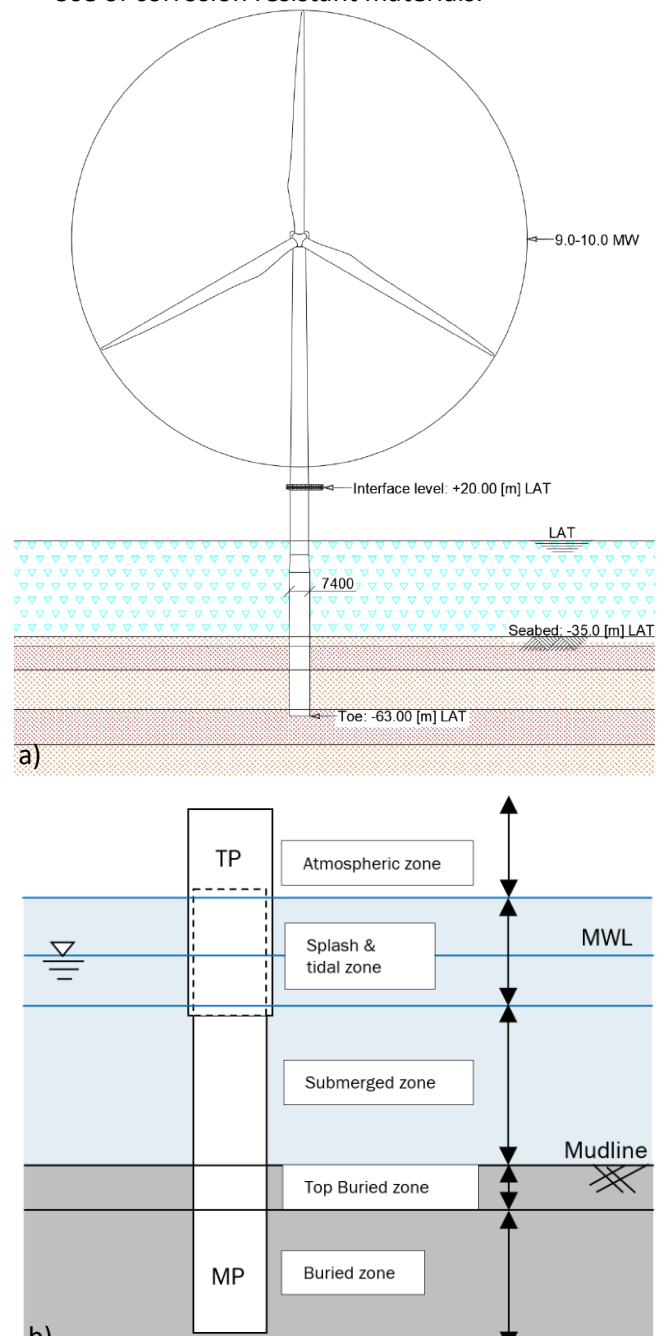


Figure 2.1 - a) Offshore wind turbine overview, b) Monopile divided into different zones to accommodate for different corrosion rates. LAT = lowest astronomical tide, MP = monopile, TP = transition piece, MWL = mean water level.





The selected measures will have impact on fatigue design of the structure due a possible change in S-N curves:

- Free corrosion curve (more steel due to corrosion allowances),
- In air curve (relies on presence of intact coating),
- Cathodic protection (CP) in seawater curve.

## The following coatings are considered:

- 1. No coating
- 2. Local coating around the welds only (no temporary CP);
- 3. Temporary coatings (e.g. 1 to 1.5 years, after which the CP system is activated);
- 4. Current high build epoxy systems, such as Norsok M501 system 7a [4], up to 15 years useful life in splash zone can be assumed
- 5. Glass-flake / polyester systems: up to 20 years (acc. DNV-RP-0416 [5]);
- 6. Full lifetime. Although lifetime definition is also variable to change (+/- 25 years for projects currently, but for instance new permits are allowing to extend to 40 years in NL);
- 7. Thermal sprayed aluminium (TSA) or zinc aluminium (TSZA) coatings can offer long lifetime, however currently only feasible on outside of piles and on flanges for relatively large surfaces (automated spray systems not yet available for internal and health/safety considerations).

Figure 2.2 shows a monopile with only the welds being coated for corrosion protection. Figure 2.3 shows a monopile with a full coating system (primer and top layer) at the top of the pile (yellow), a thermal sprayed aluminium (TSA) layer in the middle part, and only the welds being coated for the buried zone.



Figure 2.2 – Monopile with only the welds being coated for corrosion protection. Courtesy to Sif and Van Oord Offshore Wind.

A cathodic protection system is only effective from lower splash zone until the top of the buried zone. Possible systems (external and/or internal) are:

- 1. None
- 2. Galvanic anode corrosion protection (GACP);





3. Impressed current cathodic protection (ICCP).

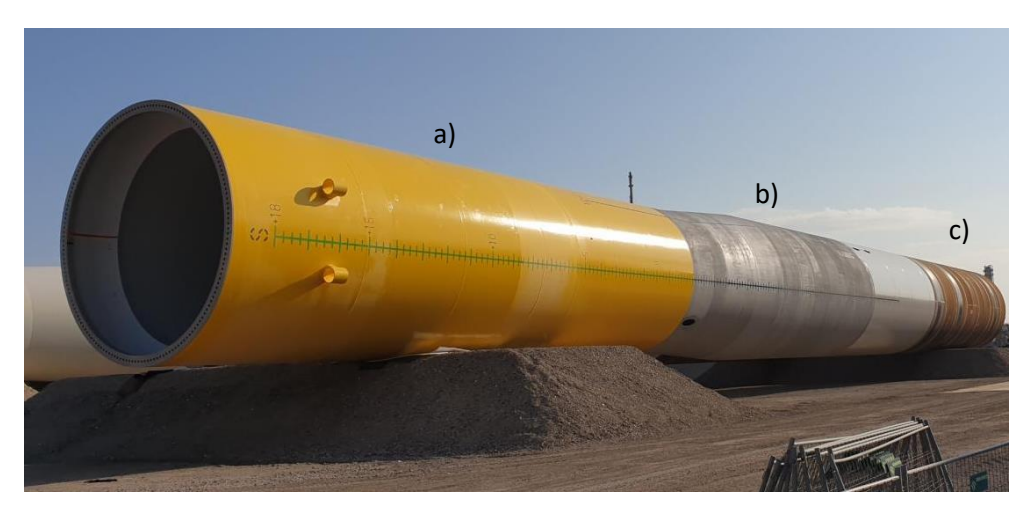


Figure 2.3 – a) Coating, primer and top layer, (yellow), b) Metallisation with a TSA (thermal sprayed aluminium) layer, c) Only the welds have been coated. Courtesy to Sif and Van Oord Offshore Wind.

Table 2.2 gives the scenarios of corrosion mitigation strategies considered in this project [21]. Scenario 0 is a base scenario, in which no corrosion mitigation techniques are applied, resulting in free corrosion in all zones. Scenario 1 to 3 consider a coating in the atmospheric and splash & tidal zone, and no coating in the buried zone. The corrosion mitigation techniques in the submerged zone and top 3 m of the buried zone are equal for each scenario. In scenario 1 to 3, an impressed current cathodic protection (ICCP) or galvanic anode cathodic protection (GACP) system is applied. In scenario 1, there is no coating applied, where in scenario 2 the welds are coated, and in scenario 3 all material is coated in the submerged zone and top 3 m of the buried zone. In scenario 1, the period between installation of the monopile, and installation of the tower is varied. It is assumed that at the moment the tower is installed, the ICCP system is installed too. For all other scenarios, it is assumed that the tower and ICCP system are installed 1.5 years after the monopile.

The following assumptions are made with regard to these corrosion protection scenarios:

- The lifetime of the structure to be considered equals 30 years.
- The lifetime of the coating to be considered is 15 years in the splash & tidal zone and top 3 m of buried zone, and 30 years in the atmospheric zone and submerged zone.
- Within the lifetime of the coating, the coating remains fully intact.
- The lifetime of the cathodic protection (ICCP or GACP) system to be considered is for the full lifetime of the structure.
- It is assumed that a ICCP or GACP potential of -800 mV can be generated up to a depth of 3 meter to provide complete protection.
- It is assumed that the ICCP system is fully active one month after installation of the tower and ICCP system.
- For all zones, it is assumed that there is free corrosion when no mitigation methods are applied.
- ➤ Welds are present in all zones. Related DNV fatigue detail categories and curves [19] to be investigated are the D-category for the as-welded welds, and the C1-category for the flush ground welds.
- Any fatigue damage due to loads during hammering and before installation of the tower is neglected.





Table 2.2 – Corrosion mitigation scenarios for the different zones of the monopile considered in this study [21].

			Scenario 1				Scenario 2	Scenario 3
		Scenario 0	A	В	С	D		
Period between installation MP (equals start of ICCP if		0 years	0.5 years	1.0 year	1.5 years	1.5 years	1.5 years	
Atmospheric zone	No Coating	Coating				Coating	Coating	
Splash & tidal zone	No Coating	Coating			Coating	Coating		
Submerged zone	External	No Coating	No Coating, GACP / ICCP	No Coating,	No Coating,	No Coating,	Only weld coating,	Coating,
Top 3 m of buried zone	External	No Coating	No Coating, GACP / ICCP	No Coating, ICCP	No Coating,	No Coating,	Only weld coating,	Coating,
Buried zone	No Coating	No Coating				No Coating	No Coating	



# 3 Deterministic Pit corrosion – fatigue model – WP2

#### 3.1 Introduction

A deterministic corrosion fatigue model is developed to determine the fatigue life of base material and welded components in steel structures incorporating the combined corrosion and fatigue degradation mechanisms. These mechanisms can synergetically act together: the corrosion process is time-dependent, the fatigue process is (stress) cycles-dependent, see Figure 3.1.

The corrosion process consists of surface film breakdown, uniform corrosion (wall thickness reduction) and pit growth.

The fatigue process consists of three phases:

- Fatigue crack initiation phase,
- Short fatigue crack growth phase,
- Long fatigue crack growth phase.

## 3.2 Model description

In this study, the short fatigue crack growth phase is incorporated in the fatigue crack initiation phase by considering the notch strain theory of 'low cycle fatigue curve'. This is further discussed in Section 3.3 in which the initiation module is discussed. The propagation module is discussed in Section 3.4.

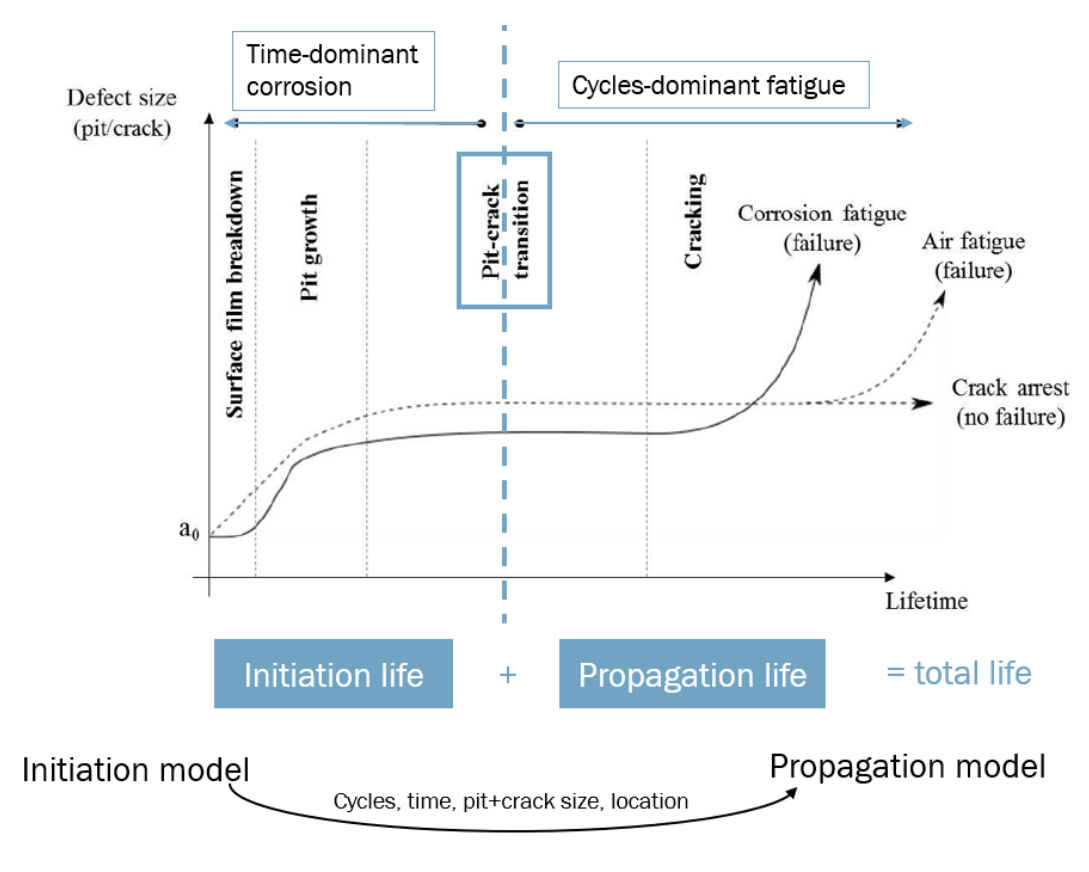


Figure 3.1 - Phases of corrosion fatigue based on Larrosa (2018) [6].

The <u>cor</u>rosion <u>fatigue</u> model ('CorFat') [9] consists of two modules: (i) the initiation model which determines the moment in time and location where a fatigue crack initiates from a corrosion pit (pit-





to-crack transition), and (ii) the propagation model which determines number of cycles from an initiated crack to failure of the structure.

#### 3.3 Model for the Pit-to-Crack Transition

Based on our analysis of all available results in literature and observations available in literature, in this project a new strategy for the prediction of the pit-to-crack transition has been developed, see Rodenburg [8] (2020).

This research presents a combined analytical/numerical model that implements mechanisms of both the fatigue and the corrosion process to determine the moment in time and location in the corrosion pit of the pit-to-crack transition. The hypothesis used to build the model is that the pit-to-crack transition occurs at the moment that a fatigue crack initiates. Assumptions are made to be able to predict the level of stress and strain at the surface and below the surface of a corrosion pit using a FEM model. Using the stress and strain levels, damage is accumulated until the failure criterion is reached, i.e. when a fatigue crack will initiate. In this research study, elliptically shaped pits are considered, with and without a certain roughness at the surface of the corrosion pit. A flowchart of the developed corrosion-fatigue model is shown in Figure 3.2.

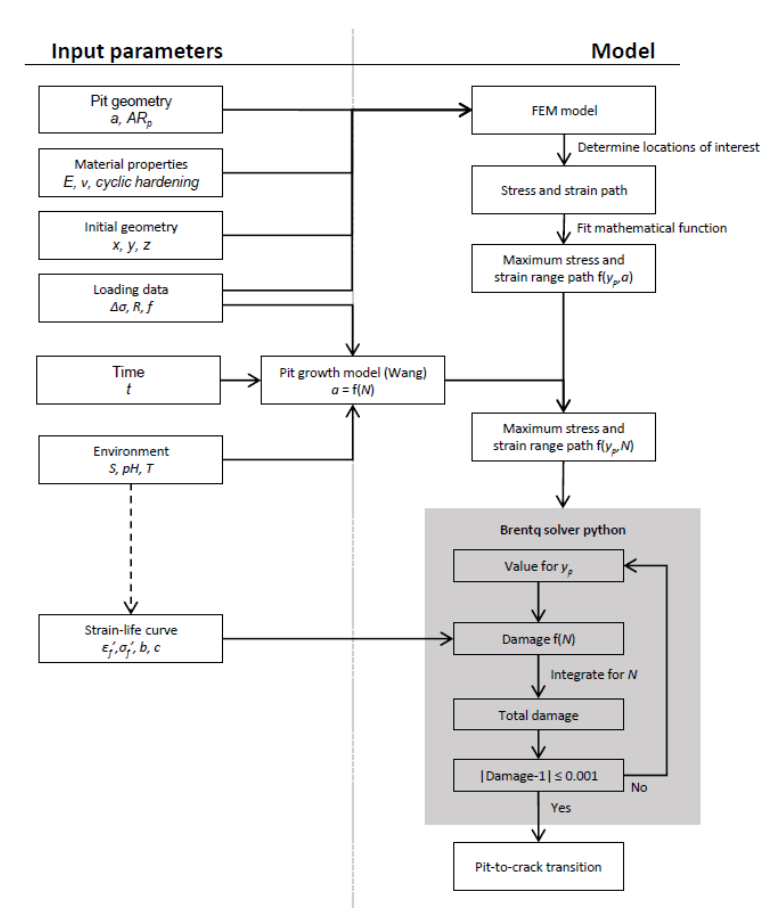


Figure 3.2 - Flowchart of the corrosion fatigue model, see Rodenburg [8].

#### 3.3.1 Initiation module

The goal of the fatigue crack initiation module is to determine the moment in time and location in a corrosion pit at the pit-to-crack transition. The pit-to-crack transition is the moment that the corrosion fatigue process will become dominated by the fatigue process instead of the corrosion process, as





depicted in Figure 3.1. Figure 3.3 shows the building blocks of the corrosion fatigue crack initiation life module. This section will discuss the building blocks in this figure.

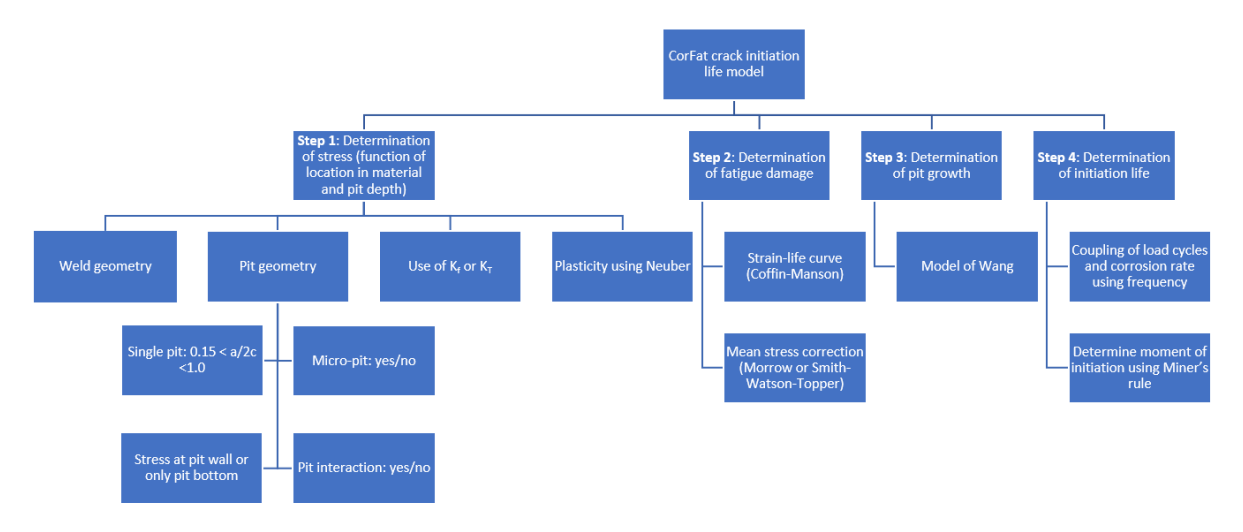


Figure 3.3 - Building blocks of the fatigue crack initiation module [9].

#### 3.3.2 Determination of stress concentration

The largest stress concentration of a typical full penetration girth weld is found at the weld toe. Therefore, in this model, it is conservatively assumed that a corrosion pit is located at the weld toe. Corrosion pits can obtain various shapes, often elliptical, in different formations, and with micro-pits present in larger pits. A different shape, formation or extra pits in the pit bottom could result in different locations where the stress concentration is largest. Also, the location with largest stress concentration is not necessarily the location where most fatigue damage is accumulated, due to the strong stress gradient influence. Therefore, different combinations of pits and different locations in and around the pit have been regarded. Corrosion pits are assumed to have a circular shape at the plate surface and an elliptical shape in thickness direction. A schematic cross-section of corrosion pits including all parameters that define the pit is given in Figure 3.4. The parameters in the figure: pit depth  $a_p$ , pit width  $c_p$ , micro-pit depth  $a_{micro}$ , micro-pit width  $c_{micro}$ , and initial centre-to-centre distance of two pits  $s_{cc.i}$ .

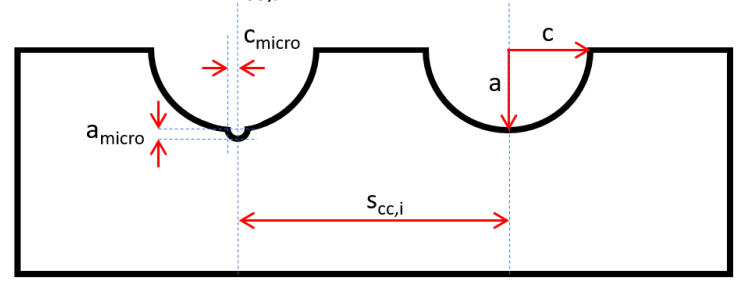


Figure 3.4 - Schematisation of corrosion pits including all parameters.

For single pits, two locations have been regarded: the pit bottom, and the pit wall. The maximum stress is found at either of these locations [8], depending on the pit shape. For double pits, two locations are regarded: the pit wall of one of the pits, and in between the two pits (this is also the location where the two pits will coincide). Figure 3.5a/b show some examples of such situations as observed in coupon exposition of steel S355NL in the North Sea [11]. Although this modelled situation of double pits can





be considered as a worst case, the probability of occurring on a monopile with tens of metres of welded length is considered as possible.



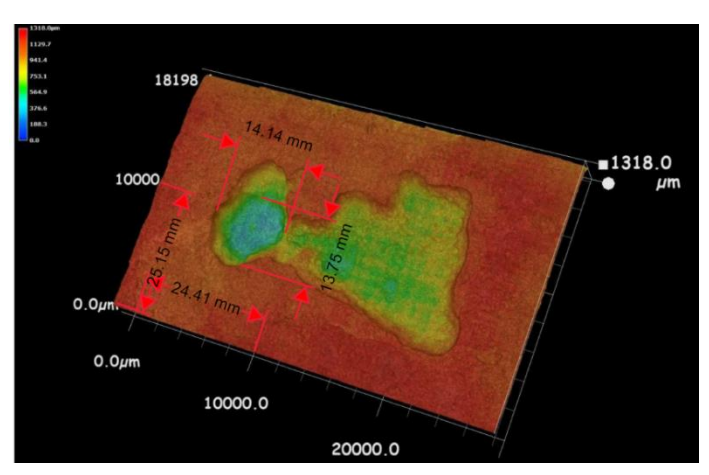


Figure 3.5a/b – Situations of corrosion pit interaction: a) a cluster of micro-pits in a macro-pit, b) a 3D scan of corrosion pits which coincide. Results of coupon exposition data of steel S355NL exposed inside monopiles on the North Sea [11].

## 3.3.3 Pit growth determination

In free corrosion conditions, a corrosion pit will expand in time. A description of the used pit growth model to quantify pit growth in time for steel grade S355M exposed in North Sea seawater is given in the final report of work package 3 of this C-FLO project of TNO and Deltares [11].

## 3.3.4 Initiation life determination

The corrosion process (pit growth process) is time-dependent, while the fatigue process is cycles-dependent. Both processes are coupled using the loading frequency f in Hz. Using the loading frequency, the fatigue damage fraction D can be determined at each location in the material along the stress path as a function of time or cycles. To determine the moment in time (equal to a certain pit depth) a crack initiates in the corrosion pit (e.g. the pit-to-crack transition), a solver function in Python is used which determines the pit depth at which the accumulated damage equals 1.0 at the location of interest.

# 3.4 Propagation module

The fatigue crack growth up to failure of the structure is determined based on LEFM in three steps: (1) Determination of the stress intensity factor (SIF)  $K_I$ , which is the parameter that represents the stress in the crack tip, (2) determination of the fatigue crack growth rate da/dN, and (3) determination of failure of the structure.

An overview of all building blocks of the corrosion fatigue crack propagation module is shown in Figure 3.6.



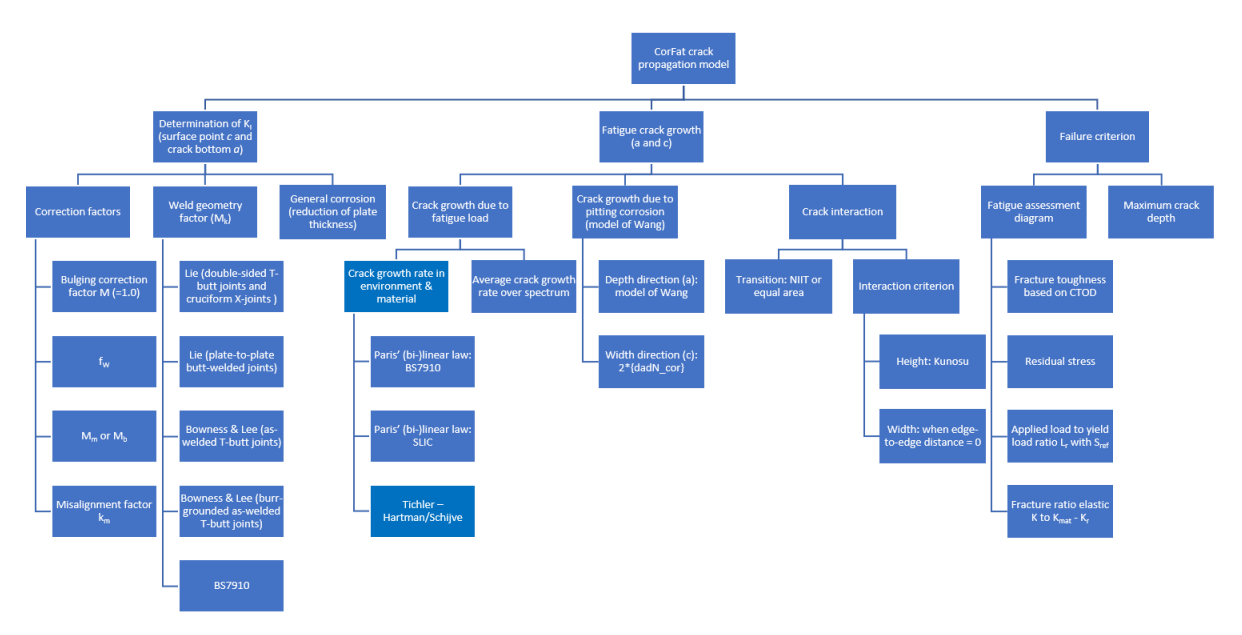


Figure 3.6 - Building blocks of the fatigue crack propagation module [9].

## 3.4.1 Pitting corrosion (competition model)

To include the effect that the corrosion pitting rate could be higher than the fatigue crack growth rate, the competition model of Kondo (see Appendix A in TNO-report [9]) is implemented. The philosophy of the competition model is given by Equation 3-1 and Equation 3-2. The pit growth rate is determined based on the model given in the final report of work package 3 of this C-FLO project of TNO and Deltares [11].

Corrosion dominates 
$$\left(\frac{da}{dN}\right)_{fatigue} < \left(\frac{da}{dt}\right)_{pit\ growth} \frac{1}{f}$$
 Equation 3-1 Fatigue dominates 
$$\left(\frac{da}{dN}\right)_{fatigue} > \left(\frac{da}{dt}\right)_{pit\ growth} \frac{1}{f}$$
 Equation 3-2

## 3.5 Input parameters

## 3.5.1 Pit corrosion

In the final report of work package 3 of this C-FLO project "Pit corrosion examinations in C-FLO WP3 - Quantification of the pit growth rate and pit shape in different seawater environments" of TNO and Deltares [11], the input parameters for the pit corrosion, pit aspect ratio and general corrosion have been defined. All these input properties for steel grade S355M exposed in North Sea seawater have been based on performed corrosion experiments, biologically induced corrosion experiments, exposed S355M steel coupons in the inner environment of monopiles located in the North Sea, and experimental programs given in literature.

# 3.5.2 Geometry

- ➤ Plate geometry The wall thickness of the monopile differs per level. This is given in WP4 of the C-FLO project.
- ➤ Weld geometry Both base material as welds are regarded (B1-, B2, C-, C1-, and D-category according to DNV-RP-C203). The weld geometry differs per level in the monopile and is given in WP4.





## 3.5.3 Crack initiation

The fatigue behaviour of steel is dependent on the environment. Therefore, curves are defined for three different environments relevant for offshore monopiles:

- Air,
- · Seawater free corrosion condition,
- Seawater with cathodic protection of -850 mV.

Figure 3.7 gives the strain-life curves for fatigue life to a very small crack.

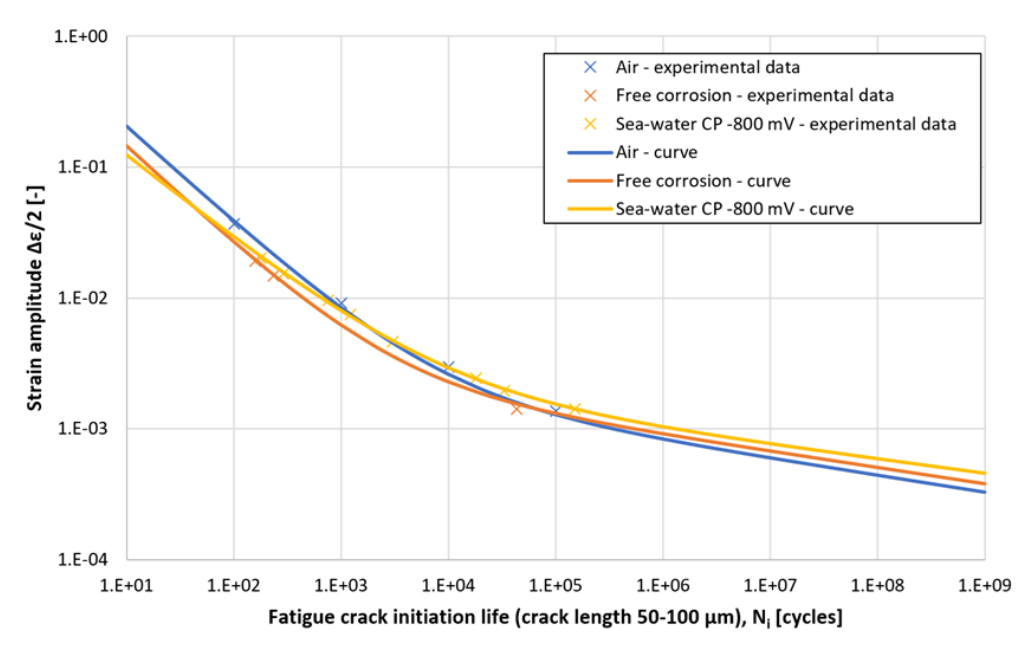


Figure 3.7 - Strain-life curves as calibrated from literature results [9] for fatigue life to a very small crack (not to failure).

## 3.5.4 Crack propagation

The used fatigue crack growth curves in this C-FLO project have been based on experiments using steel grade S355J2+N in air and seawater (free-corrosion) as performed in the SLIC project by Adedipe & Brennan et al. [16].

Figure 3.8 shows the fatigue crack growth curves for the different environments investigated in this study.



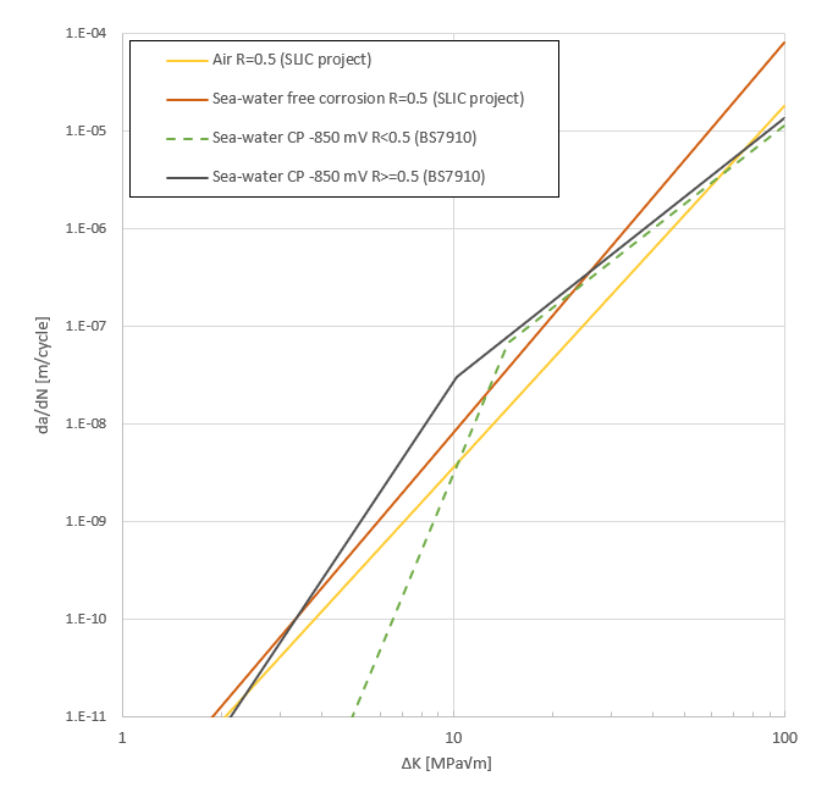


Figure 3.8 - Mean fatigue crack growth curves

A final crack length of 60% of the wall thickness is chosen as failure criterion. This corresponds to a crack width of around 45 mm, which equals a final crack aspect ratio of 0.43.

## 3.6 Conclusion

This chapter presents a deterministic corrosion fatigue model, that is developed to determine the fatigue life of base material and welded components in steel structures incorporating the combined corrosion and fatigue degradation mechanisms. The model is based on various stages of degradation, uniform and local corrosion, transition from corrosion pit to fatigue crack through crack initiation and propagation. The input parameters to the model reflect both geometrical aspects, describing the pit shape evolution as well as the influence of welds resulting in local stress concentrations, as well as typical material parameters, reflecting the resistance to corrosion and fatigue.

# 4 Fundamental pit corrosion & mechanical loading model – WP2

## 4.1 Introduction

Extensive corrosion pit growth modelling and corrosion pit growth modelling in a mechanical loaded steel specimen has been performed at the Faculty of Civil Engineering and Geosciences of Delft University of Technology under the supervision of dr.ir. L.J. Sluys, see references [17], [18].

## 4.2 Corrosion pit growth & mechanical loading modelling

## 4.2.1 Introduction

Fayezioghani et al. [18] 2022, show that a stress corrosion model for pit growth should:

a) accurately consider the electrochemistry of the corrosion process,





- b) properly deal with the moving interface between solid and electrolyte, and
- c) effectively incorporates the synergism between corrosion and mechanical field at the interface.

In Part II [18], the influence of mechanical loading is added to the approach described in Part I [17]. Part II investigates the model's capabilities of simulating stress corrosion via a set of numerical examples of corrosion pitting which include experimental validation and uncertainty quantification of model parameters and properties.

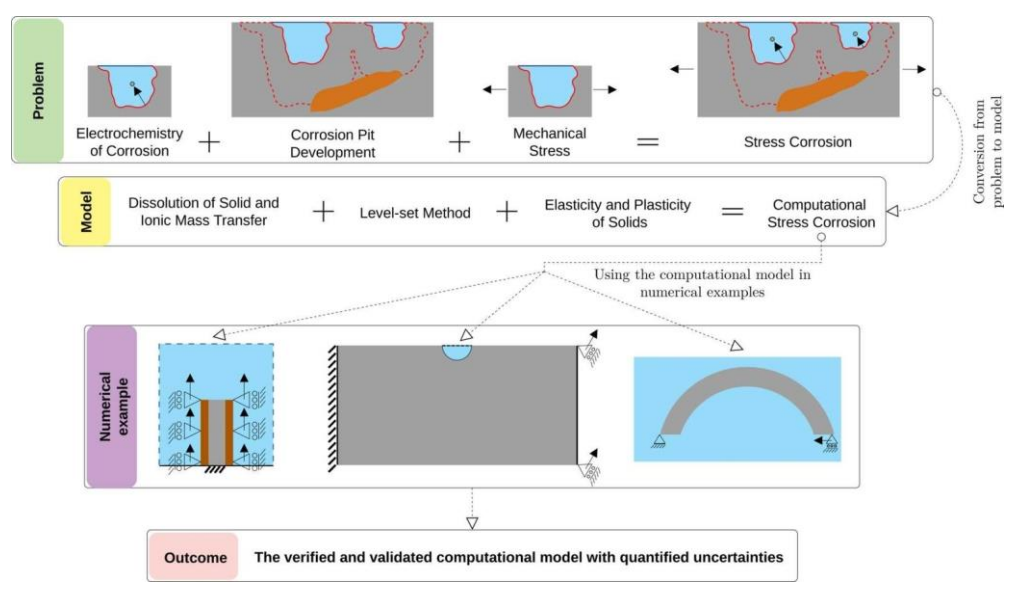


Figure 4.1 - Short overview of the stress corrosion situation, the modelling approach and the results. From Fayezioghani et al. [18].

#### 4.2.2 Example 1— Two-dimensional corrosion pit growth test with mechanical load

This example is designed to simulate the dissolution of metal into an aqueous NaCl solution in a two-dimensional corrosion pit subjected to mechanical loads. See Figure 4.2 for a schematic illustration of the specimen. The simulations are performed with a current density 1.0 mA/mm<sup>2</sup>.

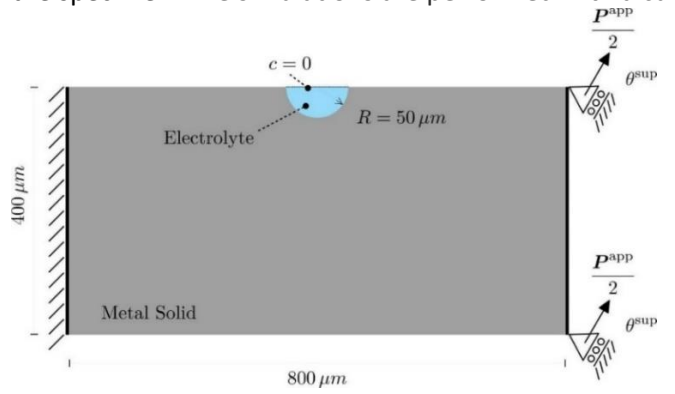


Figure 4.2 – A schematic of the 2-D pit growth with mechanical load. The initial semi-circular corrosion pit is located in the top surface of the specimen. The solid is fixed at its left edge and can freely move by a rigid body displacement in an angle  $\theta^{sup}$  at its right edge. The force  $P^{app}$  is applied with an angle  $\theta^{sup}$ , too.

Figure 4.3 shows the contour maps of metal ion concentration and mechanical multiplier in the electrolyte and solid, respectively. It presents a comparison of the interface and notch evolution of the specimen for different load types. The notch initiates from the bottom-right region of the interface where the mechanical multiplier is localized.



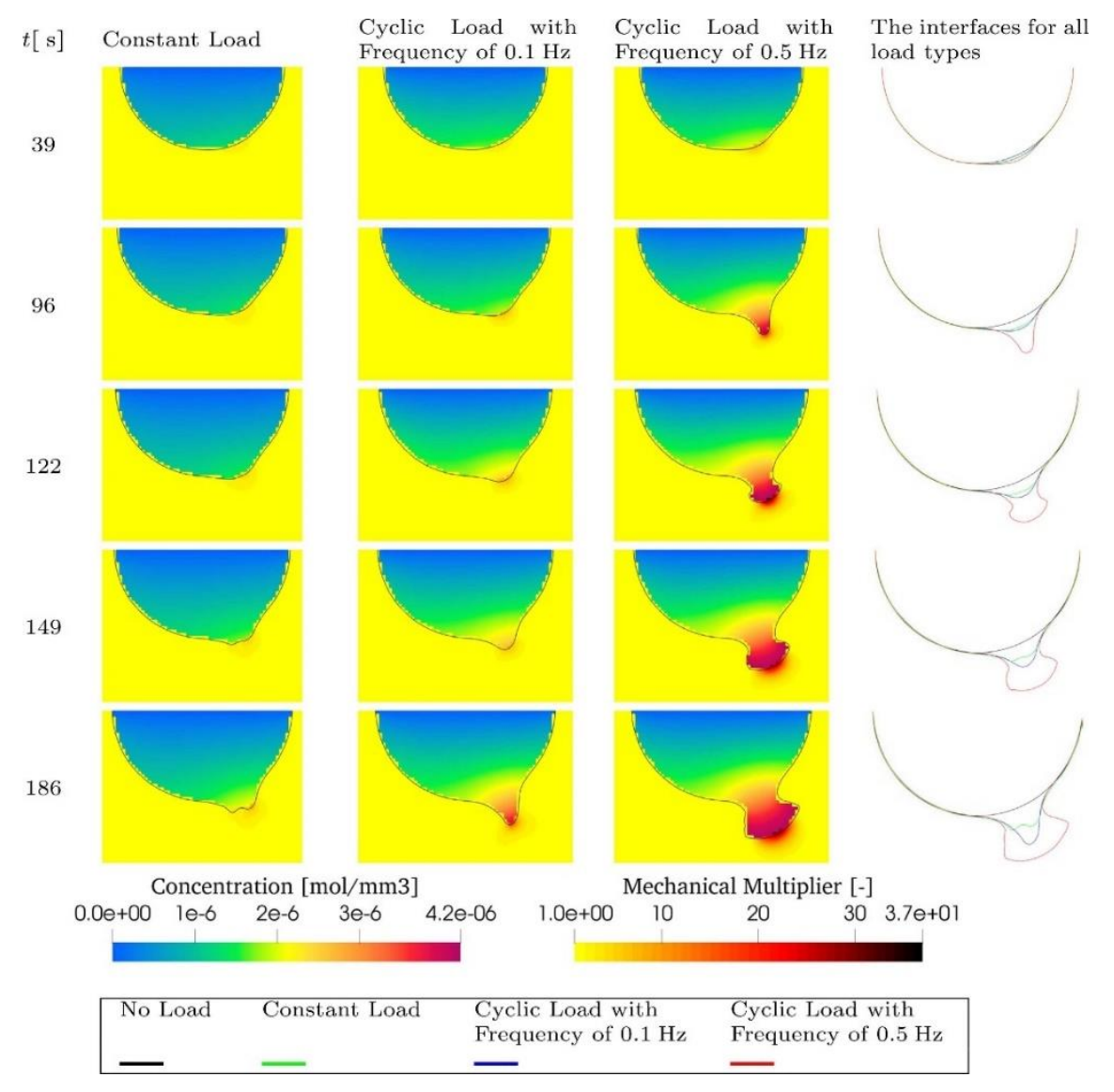


Figure 4.3 – Zoomed views of the corrosion pit and the notch at its bottom in the two-dimensional corrosion pit growth test with mechanical load example for different load types at selected times. Contour maps of the metal ion concentration and the local mechanical multiplier are illustrated in the electrolyte and solid domain, respectively. The solid bold black line indicates the interface in the contour maps. The notch initiates from the bottom-right region of the interface and grows faster as time proceeds.

## 4.2.3 Example 2 - C-ring test

The C-ring test is a test provided by international standards for stress corrosion of metals and alloys. Figure 4.4a shows the geometry and dimensions of the specimen. In literature experimental results of stress corrosion tests with Q345R steel by this test have reported pit/crack length evolution which is utilized for calibration and validation in this numerical example. In the test, a constant displacement is exerted to the specimen by a bolt passed through the 6 mm-diameter hole, and the specimen is immersed into hydrofluoric acid. The experimental results show that the free corrosion weight loss of the specimen is almost constant, which is an appropriate characteristic for the assumption of constant overpotential-induced electric current surface density in this paper.





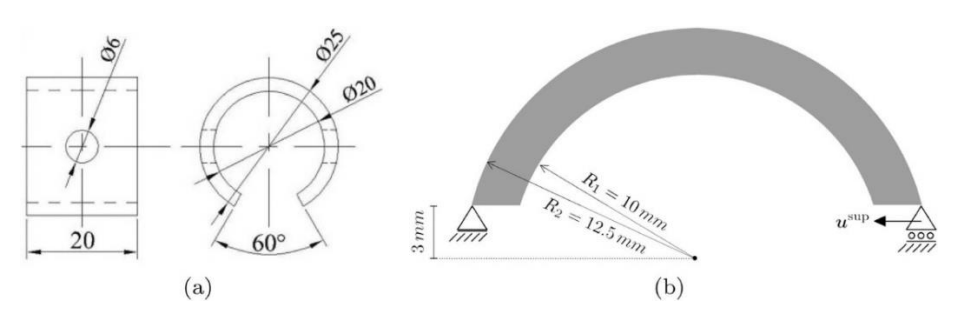


Figure 4.4 - The C-Ring test set-up: a) geometry and dimensions in mm and b) computational geometry and boundary conditions.

The pit depth is plotted versus time for the two loading cases in Figure 4.5. As pointed out in [18], the constant surrounding corrosion speed is assumed to be 0.450 and 0.238  $\mu$ m/min for  $\sigma_t$  = 0.80 $\sigma_y$  and 0.55 $\sigma_y$ , respectively. Furthermore, the nonlocal length scale as well as parameters for the scalar plastic strain measure are calibrated based on the experimental results related to  $\sigma_t$  = 0.80 $\sigma_y$ :  $e_{th,1}$  = 0.0035 and  $e_{th,2}$  = 0.0280. Then, they are validated for the experimental results related to  $\sigma_t$  = 0.55 $\sigma_y$ . The figure shows that the simulations are in good accordance with the experimental data. In addition, the numerical results depict that the proposed strain measure can appropriately be employed to model the accelerating and decelerating experimental pit depth growths.

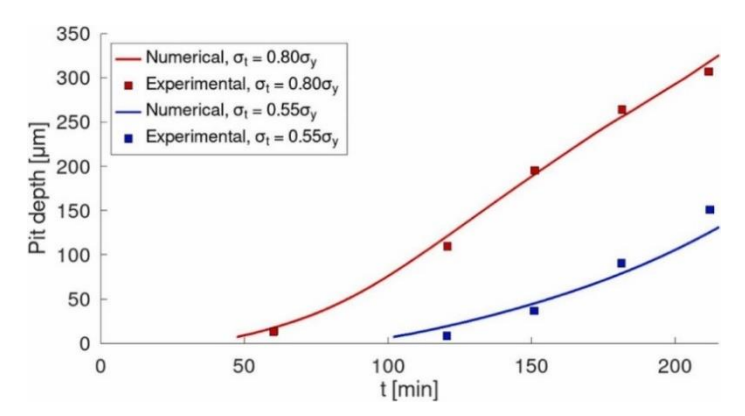


Figure 4.5 - The pit depth evolution in the C-ring test example. The numerical depths show good accordance to experimental data.

## 4.3 Conclusion

This chapter provides background to a fundamental approach towards modelling extensive corrosion pit growth and corrosion pit growth in a mechanically loaded steel specimen. The modelling approach is illustrated by two examples: 1) A two-dimensional corrosion pit growth test with mechanical load and 2) a C-ring test.

## 5 Experimental results - WP3

#### 5.1 Introduction

To calibrate parameters that are input to the deterministic corrosion fatigue model as presented in Chapter 2, three sources have been used: 1) Field data have been studied that focussed on pit corrosion as measured on coupons that were exposed in the vicinity of offshore monopiles; 2) Experiments have been performed to determine pit corrosion rates with and without MIC conditions; 3) Literature data have been analysed. This chapter summarises the analysis of the field data and experimental results, as carried out in C-FLO WP3.





#### 5.2 Pit corrosion – exposure of coupons in offshore monopiles

Two datasets of steel coupons which have been immersed in the seawater inside different monopiles of wind turbines in the North Sea for periods between 87 and 1052 days were available. The coupons were made of structural steel S355NL, with dimensions of  $100 \times 150 \times 5$  mm, and exposed at different levels in the monopile.

Dataset A consists of 200 coupons which were divided over 25 wind turbines with an exposure time varying between 384 and 605 days and dataset B consists of 161 coupons with an exposure time varying between 331 and 1052 days.

## 5.2.1 Local corrosion

The photo in Figure 5.1 shows a cluster of microscopic pits and the maximum depth of penetration is given to be  $0.25 \pm 0.05$  mm.



Figure 5.1 – Cluster of microscopic pits on surface, maximum depth of penetration estimated at  $0.25 \pm 0.05$  mm. The method of assessing the pit dimensions for dataset A is shown (magnification estimated on basis of hole size of 12 mm).

## 5.2.2 Local corrosion shapes and distribution

The corrosion pit aspect ratio (a/2c) is the ratio of the maximum pit depth (a) divided by the minimum pit width at the surface (2c). With this ratio the pit shape has been characterised. A histogram of the corrosion pits with the aspect ratio of the pit is shown in Figure 5.2. For the distributions shown in the histograms in Figure 5.2 it should be noted that the small and very small pits from both datasets have not been measured and characterized.





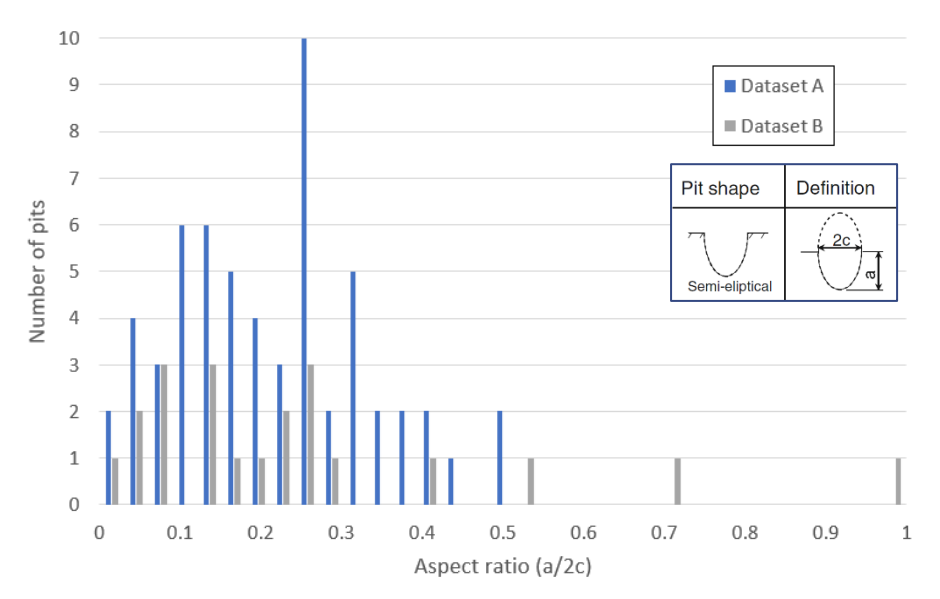


Figure 5.2 – Histogram with the aspect ratios of the corrosion pits. (The x-axis is limited to 1.0, where dataset A contains one pit aspect ratio of 1.6. This point is excluded from the graph to make it more readable.)

In these corrosion pits often small, so called "micro-pits" can be identified. Figure 5.3a/b shows an example of a micro-pit present in a (macro) corrosion pit.

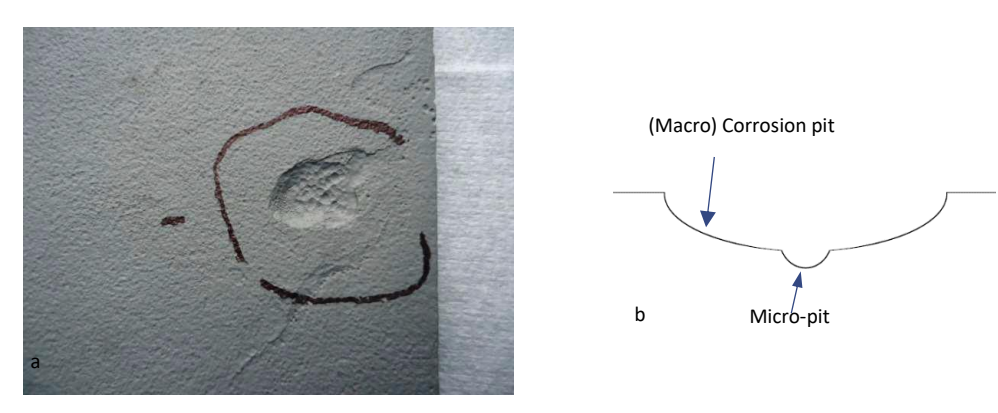


Figure 5.3a/b – Micro-pits present in a (macro) corrosion pit, a) coupon with area of localised corrosion attack – depth 0.92 mm, b) schematic.

Figure 5.4 shows two examples of clusters of micro-pits within a large corrosion pit. Typically shallow pits include clusters of micro-pits. All pits including micro-pits contain multiple micro-pits, thus interaction between micro-pits is present. Different situations of micro-pit distributions have been identified. Isolated pits, clustered pits, and micro-pits all over the coupon have been observed.





Figure 5.4 – Example of clusters of micro-pits within a large corrosion pit.

## 5.3 Exposure & measurements in microbiologically enriched seawater

#### 5.3.1 Introduction

Microbiologically Influenced Corrosion (MIC) was studied in bioreactors with ER probes, coupons and C-rings, and dogbones, see Deltares report of Jansen et al. [10]. Different methods for exposure of steel in microbiologically active seawater were used:

- 1. ER probes in bioreactors, see Figure 5.5a,
- 2. Coupons, C-rings and ER probes in vessels, see Figure 5.5b,

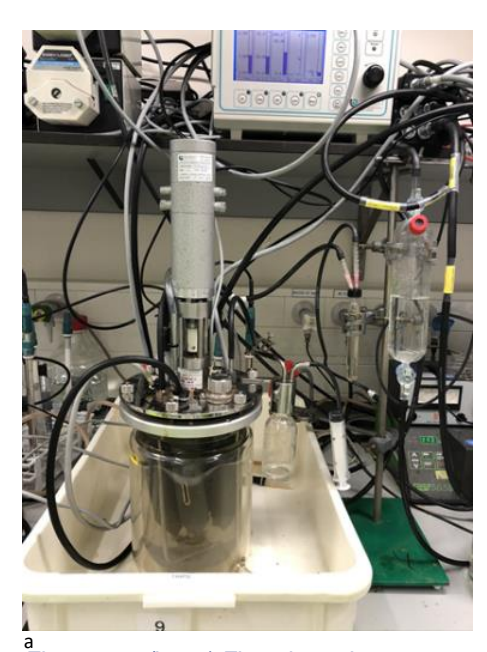




Figure 5.5a/b – a) Flow-through reactor setup with ER probes; b) Stirred vessel incubation with C-rings, ER probes and steel coupons.

#### 5.3.2 ER probes in bioreactors

The most notable effects of environmental conditions determined can be summarized as follows:

A. Nutrients, nitrogen (N) and phosphorus (P), are expected to have an effect on MIC rate as MIC is a biological process for which nutrients are required. A clear effect of nutrients on MIC is





shown in Figure 5.6a, but after some time at low nutrient concentrations MIC was again occurring at considerable rates. For practice, these results imply that nutrient effects are likely for start-up of MIC, but might be masked once the biofilm is established.

B. Cathodic protection (CP), Figure 5.6b shows the applied potential of –700 mV vs Ag/AgCl and more negative, corrosion rate was brought down to zero.

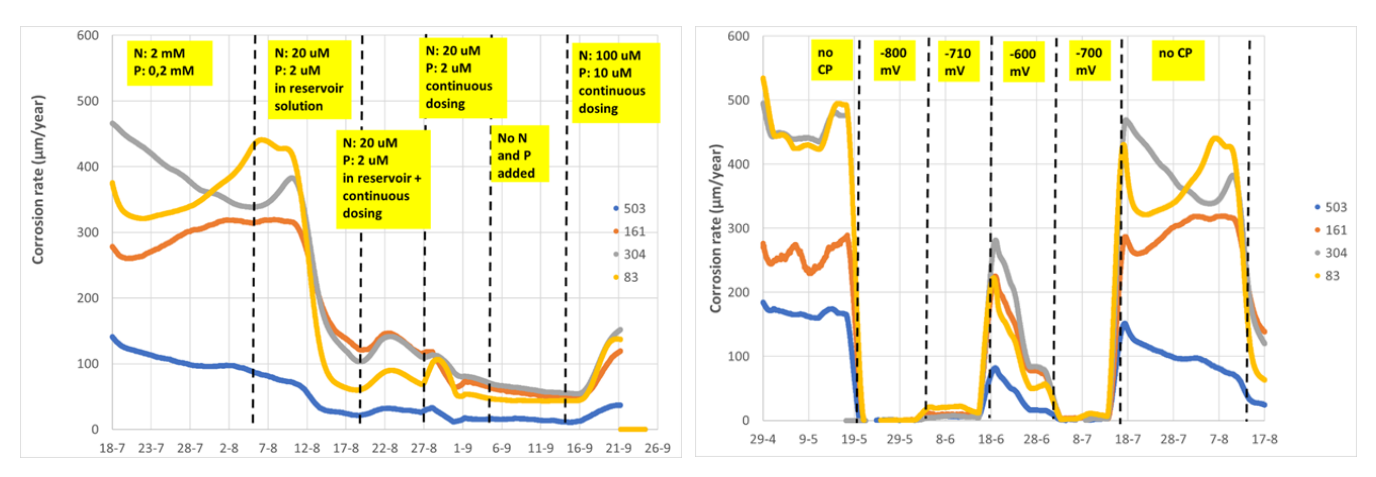


Figure 5.6a/b – a) Effect of nutrients (N and P) on corrosion rate, b) Effect of cathodic protection on corrosion rate as a function of time (on this axis the date is shown).

#### 5.3.3 Coupons, C-rings and ER probes in vessels

After long term exposure on dogbones, C-rings and coupons, no severe/sharp pitting was established as a result of MIC. MIC under these conditions might take longer to establish/difficult to control. ER Probes were fully corroded and various corrosion products were visible. Most of metal surface was gone: more general corrosion than pitting was found.

Corrosion rates due to MIC vary between ca 0.1 and 1.0 mm/year. An active MIC biofilm can cause MIC rates of 0.5 to 1.0 mm/year, but this is strongly dependent on the development of a MIC biofilm (which takes time, order of magnitude months to one year) and on the local conditions, which can lead to development or absence, and low or high activity of an MIC biofilm. This leads to a local and difficult to expect occurrence of MIC.

Cathodic protection is found to have a strong effect on MIC: at 700 mV vs Ag/AgCl and more negative, MIC was completely stopped. On the other hand, from earlier research it is known that established MIC biofilms can withstand negative elevations of CP. These data were collected for groundwater conditions and it remains to be tested whether this can be the case for seawater environments as well.

## 5.4 Exposure of coupons in artificial seawater (without MIC)

Samples of two S355M steel grades were submerged in slow flowing artificial seawater without mechanical loading for analysis of corrosion rates and for pre-corroding dogbones to be exposed to fatigue loading (section 5.7.2). Air was slowly bubbled from below.

Tests representative of the submerged show the following. None of the base material samples (Dillinger S355ML, Posco-S355-SFG, Posco-S355-REF) show typical pitting type of attack within the tested periods, up to 4250 h (equivalent for about 6 months), although locally higher corrosion rates can be observed. For flush welded samples (Dillinger-S355ML), higher corrosion rates are generally observed in the HAZ resulting in a difference in material loss, being higher in the HAZ.

The PoscoS355-SFG material shows a more general than local corrosion response than the Dillinger S355ML.





Tests representative of the splash zone show that for both Dillinger-Hütter S355ML as Posco-S355-SFG corrosion pits start to develop.

Corrosion rates are in the same order of magnitude as those found in literature.

## 5.5 Pitting-corrosion data obtained from literature, as for welded joints

Figure 5.7a/b shows the pit depth (a) and pit aspect ratio (a/c) of steel grade S355M as a function of exposure time. The S355M steel coupons were exposed in the inner environment of monopiles located in the North Sea. The period of exposure was between 528 and 1049 days. Based on these results a relation between the corrosion pit depth and exposure time is determined.

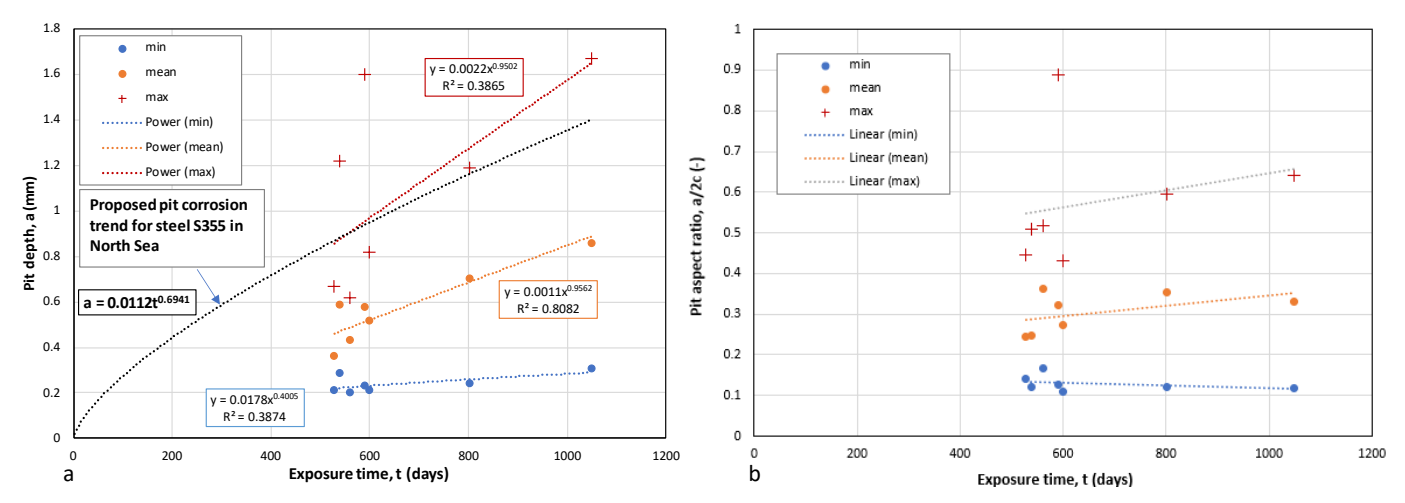


Figure 5.7a/b - a) Pit depth and b) pit aspect ratio of steel grade S355 as a function of exposure time.

Pit-corrosion rates derived from results presented in literature are given for:

- Steel grade S355M coupons exposed at different zones in monopiles in the North Sea. Corrosion rates are on average in line with findings from the field data and lab experiments.
- For the maximum pit depth in the HAZ a ratio HAZ/BM = 1.6 has been determined. For the weld metal the mean and maximum pit depth ratios are both WM/BM = 1.15.

#### 5.6 Summary of corrosion rates for various zones

A summary of pit corrosion rates for the various zones is given in Table 5.1.





Table 5.1 - Summarizing table with pit corrosion rates for linear pit growth (ranges) for base material.

		Corrosion rate without mitigation measures			
		General corrosion (mm/yr)	Localised corrosion (mm/yr)		
Atmospheric zone		0.03 - 0.06	0.10 - 0.20		
Splash & tidal zone	External	0.15 - 0.30	0.30 - 0.60		
	Internal	0.10 - 0.20	0.20 - 0.40		
Submerged zone	External	0.06 - 0.12	First 0.5 year: 0.10 – 0.20		
			After 0.5 year: 0.3 – 1.0		
	Internal	0.06 - 0.12	First 0.5 year: 0.10 – 0.20		
			After 0.5 year: 0.3 – 1.0		
Top 3 m of buried zone	External	0.02 - 0.04	First 0.5 year: 0.15		
			After: 0.50		
	Internal	0.02 - 0.04	First 0.5 year: 0.15		
			After: 0.50		
Buried zone		0.02 - 0.04	0.05 - 0.10		

#### 5.7 Corrosion-fatigue test results

## 5.7.1 Corrosion-fatigue initiation tests with artificial corrosion pits

Corrosion-fatigue crack initiation tests have been performed using specimens containing an artificial corrosion pit in artificial seawater. The objective was to determine the initiation life of these pits, more specifically the pit-to-crack transition, as a function of the fatigue stress range in a seawater environment. For these tests, a dedicated test set-up with electro-chemical instrumentation has been design and applied at TNO. An overview of the designed and applied corrosion-fatigue test set-up is shown in Figure 5.8a/b.

The round specimens had in the gauge length a diameter of 6.35 mm and were provided with an artificial corrosion pit in the middle of this gauge length. The stress concentration factor  $k_t$  = 2.8. The specimens were made of the same batch of steel S355ML. The used stress range,  $\Delta\sigma$  = 210 to 325 MPa, and stress ratio, R = 0.1.

During these tests extensive electro-chemical measurements using a dedicated potentio-static device have been performed. The normalised OCP (Open Circuit Potential) amplitudes (derived from the measured OCP) and normalised with the maximum value at final fracture as a function of the normalised test duration, are shown in Figure 5.9. Most normalised OCP curves show after a certain test duration a gradual increase. The formation of new "fresh" exposed steel crack surfaces in the used artificial seawater is assumed to be the reason for this continuing increase until the final specimen failure, see MSc report of Jamar [13].









Figure 5.8a/b – a) Overview of the corrosion fatigue test set-up. The specimen and container with artificial seawater are shown, b) specimen was, with the exception of the artificial corrosion pit, fully covered with an isolating coating to gain the highest measuring sensitivity for small crack extensions.

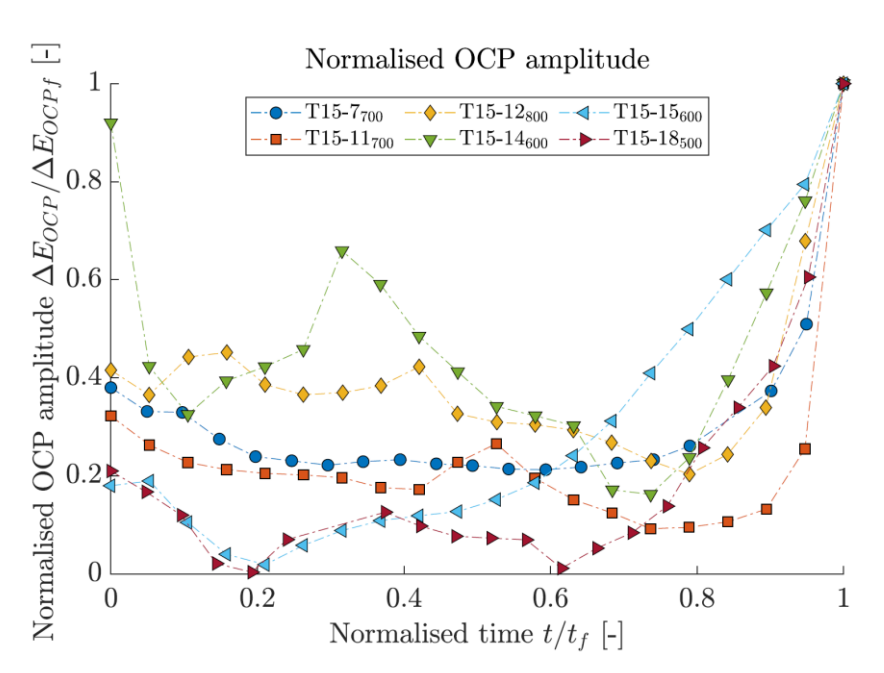


Figure 5.9 – The from the measured OCP (Open Circuit Potential) derived OCP amplitude normalised with the maximum value at final fracture as a function of the normalised test duration.

The <u>corrosion-fatigue crack initiation life</u> has been determined for an estimated life up to a crack size of approximately  $a = 100 \mu m$ . Figure 5.10 compares the test results with results obtained by Bignonnet





et al., see TNO/Deltares report [12]. The results have been adjusted to R = 0.1 for comparison based on the C-FLO model.

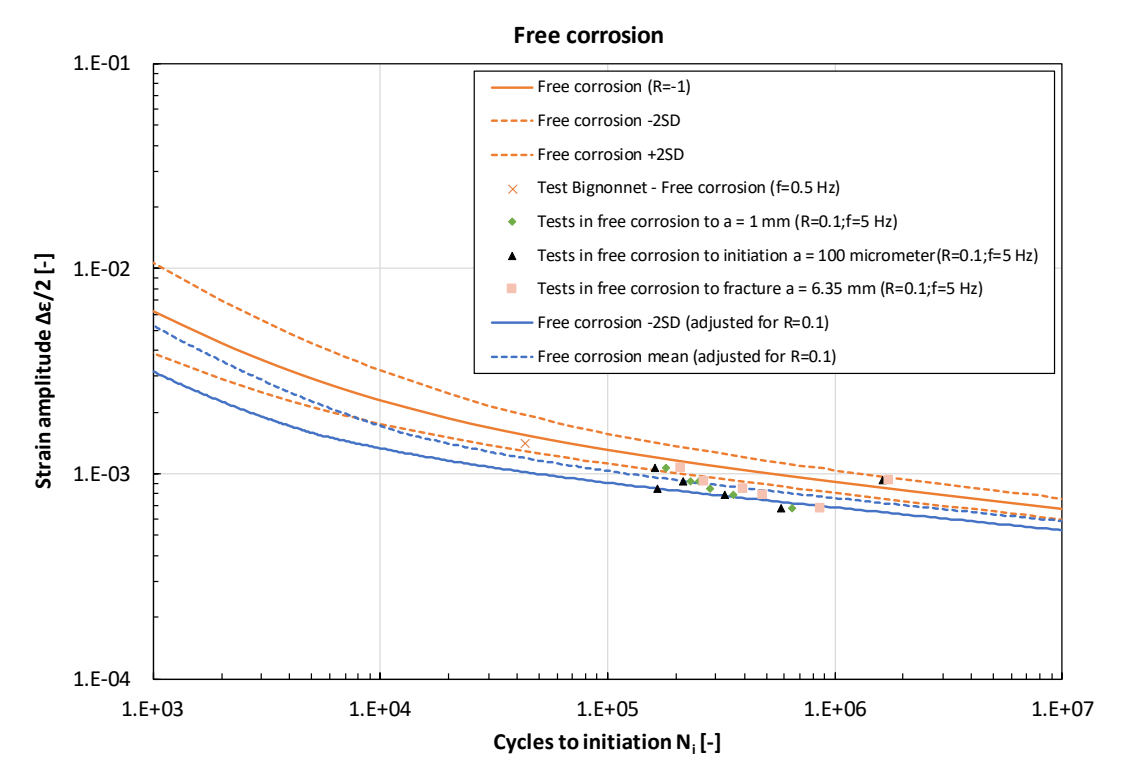


Figure 5.10 – Fatigue life to initiation ( $\sim$ 100  $\mu$ m), 1 mm crack size and to failure (fracture) of the specimens S355ML in free corrosion with artificial corrosion pit compared to results of Bignonnet et al., see TNO/Deltares report [12].

## 6 Corrosion-fatigue tests on dogbone coupons at Vattenfall

#### 6.1 Introduction

To get reliable corrosion-fatigue life data for the steel grades and welding procedures used for offshore wind piles and foundations, corrosion-fatigue tests with pre-corroded specimens have been performed in artificial seawater in a specially designed and built test setup by Vattenfall.

About 60 specimens have been manufactured of base material and welded steel S355 supplied by Dillinger Hütte (S355ML) and Posco in two grades, with a fine grained surface layer (G1), and a normal condition (H1).

Figure 6.1 shows the used specimens with the shape of a "dogbone". In the gauge length the specimens have been pre-corroded, at one side of the specimen, over an area of about 20 x 30 mm<sup>2</sup>. A part of the specimens has been pre-corrosion in artificial seawater and another part in biologically enriched artificial seawater to introduce a certain type of MIC (micro-biological induced corrosion).

## 6.2 Test set up

A new corrosion-fatigue test rig has been designed and manufactured by Vattenfall AB in Älvkarleby (Sweden) for these tests. Figure 6.2 shows a schematic of this test setup. A picture of the specimen arrangement forming a long chain is shown. The total length of the chain with dogbone specimens is about 5.5 meter. Figure 6.3 shows a picture of the test rig at Vattenfall.





The following test conditions have been used for these corrosion-fatigue test:

- 1. Environment: artificial seawater, temperature, T ≈ 20 °C,
- 2. Test frequency, f = 0.4 Hz,
- 3. Stress range,  $\Delta \sigma$  = 270 MPa, Stress ratio, R = 0.1.

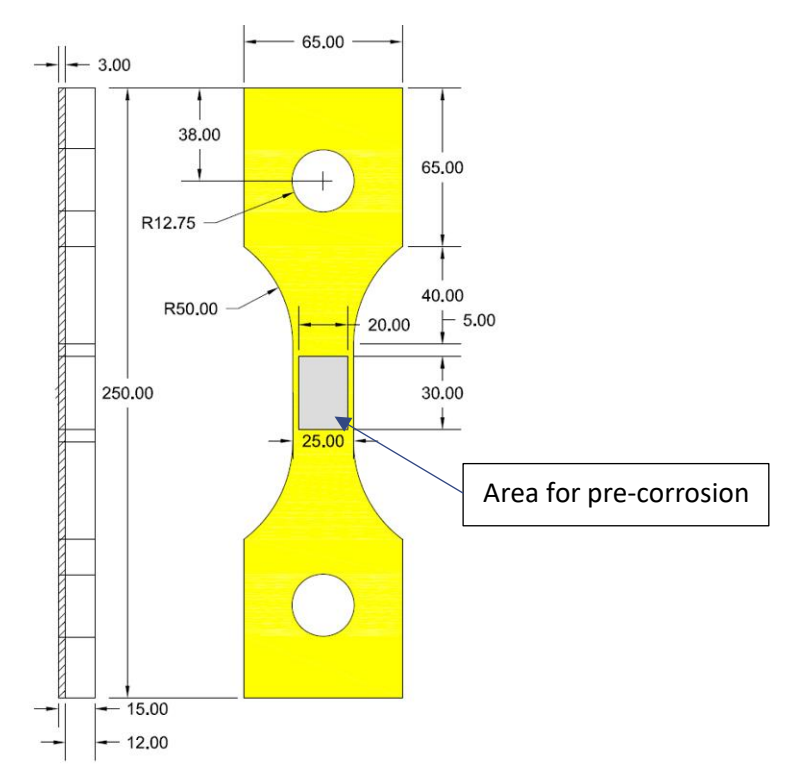


Figure 6.1 – Drawing of the specimens with the shape of a "dogbone".





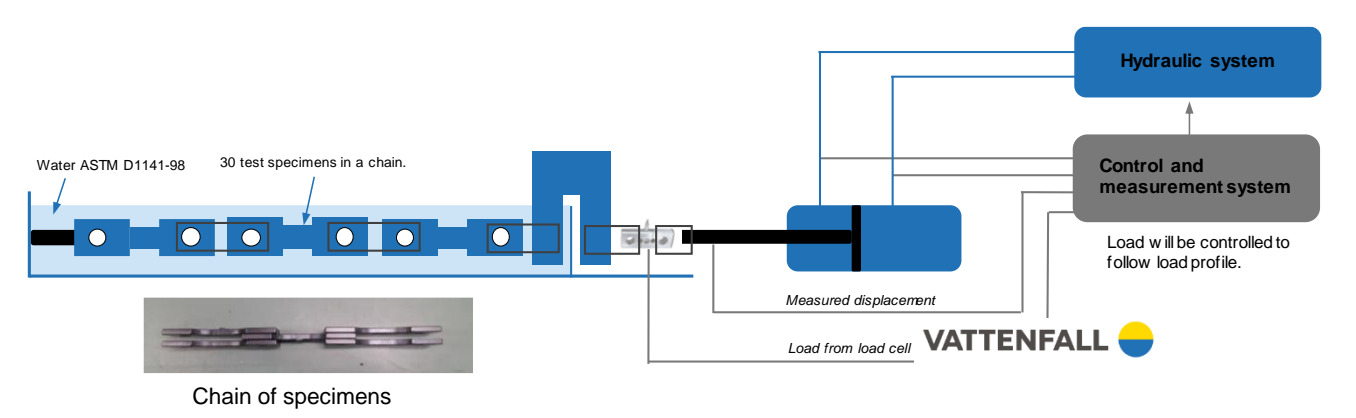


Figure 6.2 – Schematic of the corrosion-fatigue test rig designed and manufactured by Vattenfall AB in Sweden.



Figure 6.3a/b – The corrosion-fatigue test rig at Vattenfall AB in Sweden.

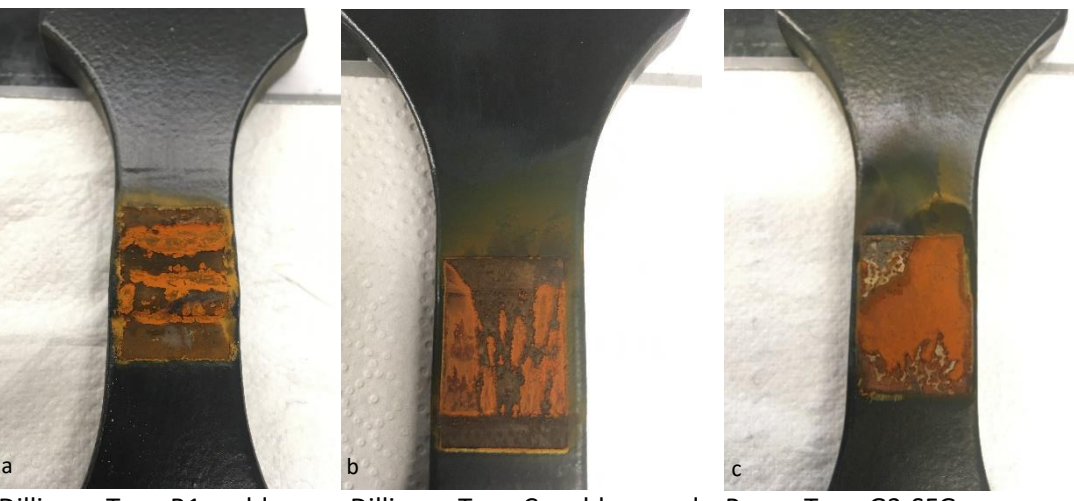
# 6.3 Pre-corrosion of specimens

A part of the specimens was pre-corrosion in artificial seawater. An extensive description of the used procedure can be found in TNO report/ Deltares report "Corrosion - fatigue tests in different seawater environments" [12] of this C-FLO project. Some pictures of pre-corroded specimens are shown in Figure





6.4a to c: a) Dillinger-Type B1-weld, S355ML from Dillinger with butt weld, b) Dillinger-Type C-weldground, S355ML from Dillinger with butt weld ground flush, c) Posco-Type G3-SFG, S355ML from Posco, base material with a fine grained surface layer.



Dillinger-Type B1-weld

Dillinger-Type C-weld-ground Posco-Type G3-SFG

Figure 6.4a to c – Pictures of the pre-corroded areas of the specimens.

Another part of the specimens was pre-corrosion in artificial seawater enriched with micro-biological active substances as bacteria to introduce MIC. An extensive description of the used procedure can be found in TNO report/ Deltares report [12] and in Deltares report [10] of this C-FLO project. Some of these pre-corroded dogbone specimens are shown in Figure 6.5.



Figure 6.5 – Dogbone specimens pre-corrosion in artificial seawater enriched with micro-biological active bacteria.

Figure 6.6 show some detailed pictures of the pre-corroded areas of as-welded specimens.





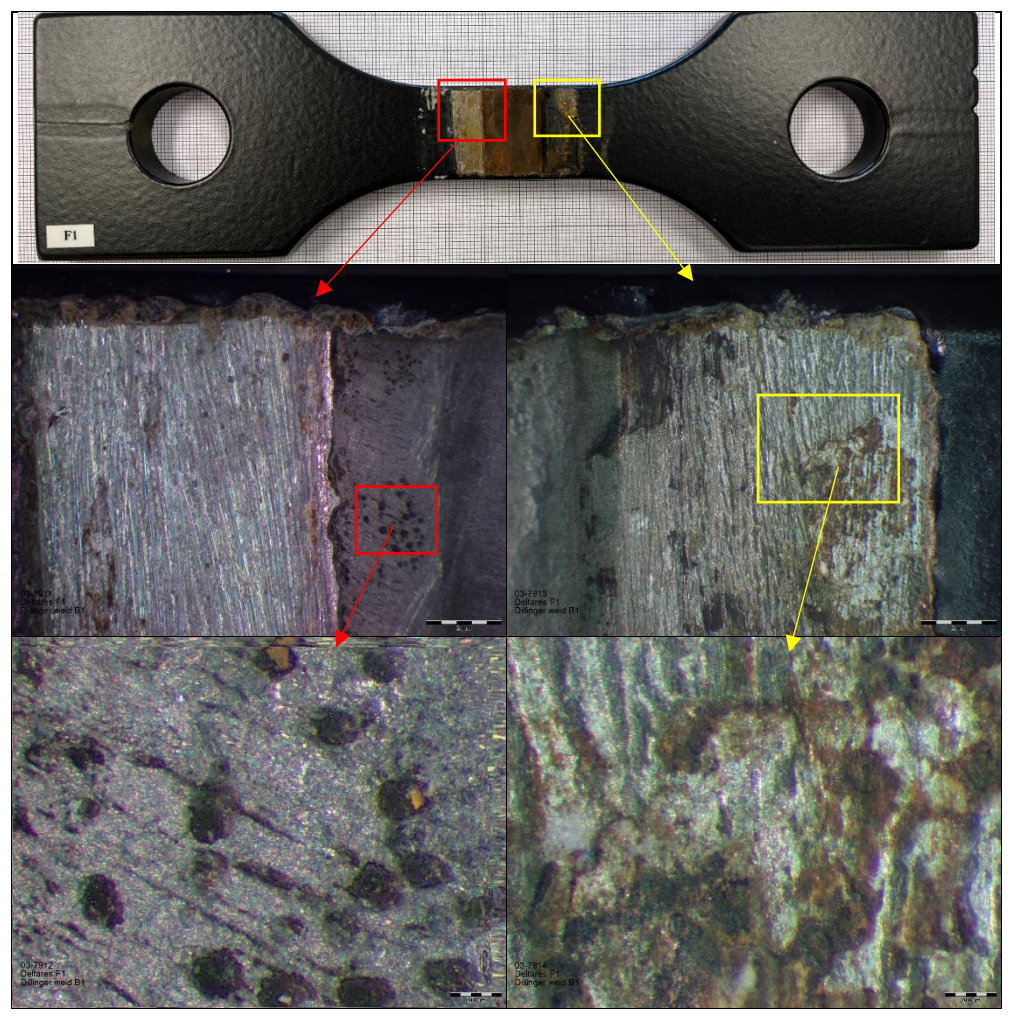


Figure 6.6 – Pictures of the attacked areas of an as-welded dogbone specimen pre-corrosion in seawater enriched with micro-biological active substances as bacteria to introduce MIC.

# 6.4 Corrosion – fatigue test results

Figure 6.7 and Figure 6.8 show examples of failed corrosion-fatigue specimens.



Figure 6.7 – Pre-corroded specimen D-B03 (E5 according Deltares) failed in the corrosion fatigue test.





Figure 6.8 – Pre-corroded specimen T-B03 failed in the corrosion fatigue test.

The results of the Vattenfall corrosion fatigue tests have been compared with predictions for the relevant geometry and environmental conditions using the C-FLO model and using the DNV RP C203.

The comparison shows that for all categories, as-welded (category D), flush-ground (Category C1) as well as base material (B2), the test results are close to or above the MEAN+2SD line estimates according to DNV RP C203.

#### 6.5 Conclusion

This chapter summarises the analysis of literature, field data and experimental results of the C-FLO project to calibrate parameters that are input to the deterministic corrosion fatigue model.

Three sources have been used: 1) Field data have been studied that focussed on pit corrosion as measured on coupons that were exposed in the vicinity of offshore monopiles; 2) Experiments have been performed to determine pit corrosion rates with and without MIC conditions; 3) Literature data have been analysed.

Corrosion-fatigue crack initiation tests has been performed using specimens containing an artificial corrosion pit in artificial seawater. During these tests extensive electro-chemical measurements using a dedicated potentio-static device have been performed. The corrosion-fatigue crack initiation life has been determined for an estimated life up to a crack size of approximately  $a = 100 \mu m$ 

Corrosion-fatigue tests with large welded specimens on dogbone coupons are executed at Vattenfall. The test results are close to or above the MEAN+2SD line estimates according to DNV RP C203. C-FLO model predictions (MEAN) are close to the experimental data. Base material from Posco shows runouts at a level of 270 MPa (>1.15 million cycles) whereas two of the reference material specimens cracked earlier.

## 7 Model results - S-N curves - WP4

#### 7.1 Introduction

The deterministic corrosion fatigue model aims at predicting the effect of structural and environmental parameters towards life assessment for optimising the structure as well as potential mitigation strategies. C-FLO work package 4 has brought the research and industrial partners together to apply





the model in various corrosion mitigation scenarios regarding the monopile to show the effectiveness of these strategies.

The following corrosion mitigation strategies have been incorporated in the model assessment: 1) coating, 2) cathodic protection and 3) free corrosion. Coating (air) environment.

In the corrosion fatigue model, the following assumptions are regarded with respect to coated surfaces or coated welds only:

- The corrosion rate for an intact coating is equal to zero.
- After a crack has initiated below the coating layer, it is assumed that the coating is also cracked. The environment in contact with the steel of the monopile is considered for the propagation life, which equals free corrosion if no cathodic protection (GACP or ICCP) system is applied.

## 7.2 Cathodic protection in seawater environment

A period of free corrosion occurs before the cathodic protection (CP) system is fully activated, except when a coating is present. In this period of free corrosion, localized corrosion, corrosion pits, can occur. When the CP system is activated, the corrosion rate is reduced to (nearly) zero, and the corrosion pits grown during the period of free corrosion remain in the structure and do not grow further during the remainder of the lifetime. Figure 7.1 gives a schematic of the change in S-N curve due to the growth of the corrosion pit (a structure with a growing notch and thus a decreasing level of the S-N curve), up to the point that the CP system is activated, after this point the S-N curve will be constant. Because this moment equals the moment that the considered fatigue load starts (the tower is installed), it is possible to generate *one* S-N curve (for the pit size at the moment de CP system is activated and from that moment on the pit growth rate is assumed to be zero) that can be used for the complete lifetime of the monopile structure.

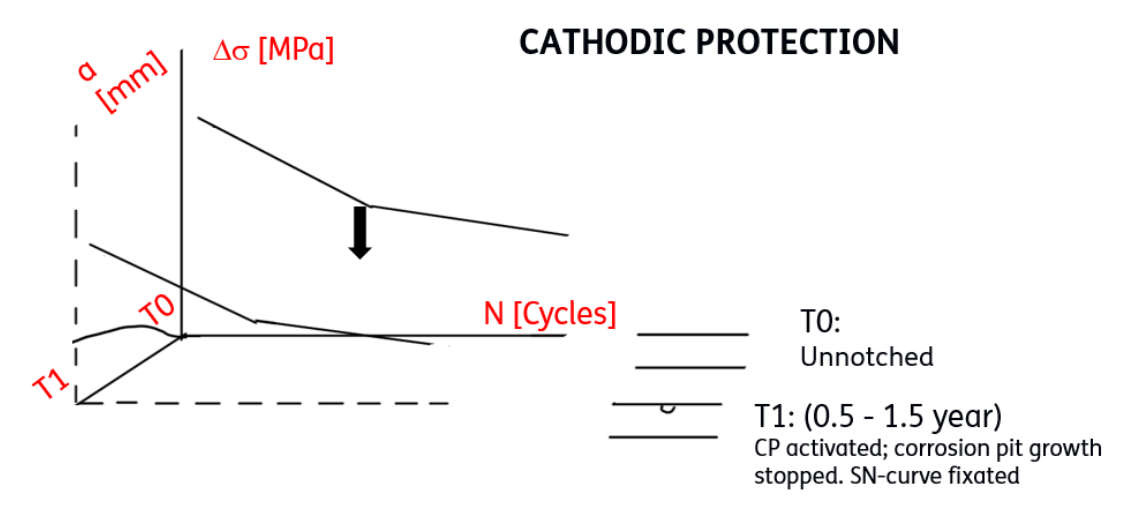


Figure 7.1 - Schematic evolution of S-N curves in zones with cathodic protection in time due to free corrosion period before activation of the CP system.

The following assumptions are made for the zones where a CP system is present:

 It is assumed that the ICCP potential of -800 mV will stop the unform corrosion and pit corrosion growth completely. This is a conservative assumption, since a very low corrosion rate could result in a larger corrosion fatigue life, due to material be taken away where fatigue damage has been accumulated.



Multiple corrosion pits can initiate in the period before activation of the CP system. It is
assumed that these pits are located at a distance from another that results in the largest stress
concentration.

## 7.3 Free corrosion environment

During free corrosion there is always a certain corrosion rate, it will never be zero. This means that local corrosion keeps developing, thus the stress concentrations in and around the pits are changing in time. Therefore, the S-N curve also shifts in time. A schematic of the evolution of S-N curves in zones with free corrosion is shown in Figure 7.2. The combination of the time-dependent corrosion process, and the cycles-dependent (time divided by frequency) fatigue process, makes it impossible to include both processes in a single S-N curve. Therefore, no S-N curves are generated for zones where free corrosion conditions occur after installation of the tower (i.e. start of fatigue load). This concerns all zones for scenario 0, and the splash & tidal zone and buried zone for scenario 1 to 3. For these zones and scenarios, the fatigue life is calculated in the corrosion fatigue model using an iterative process. For more details, see TNO-report [21] (Appendix II in Van Oord report [24].

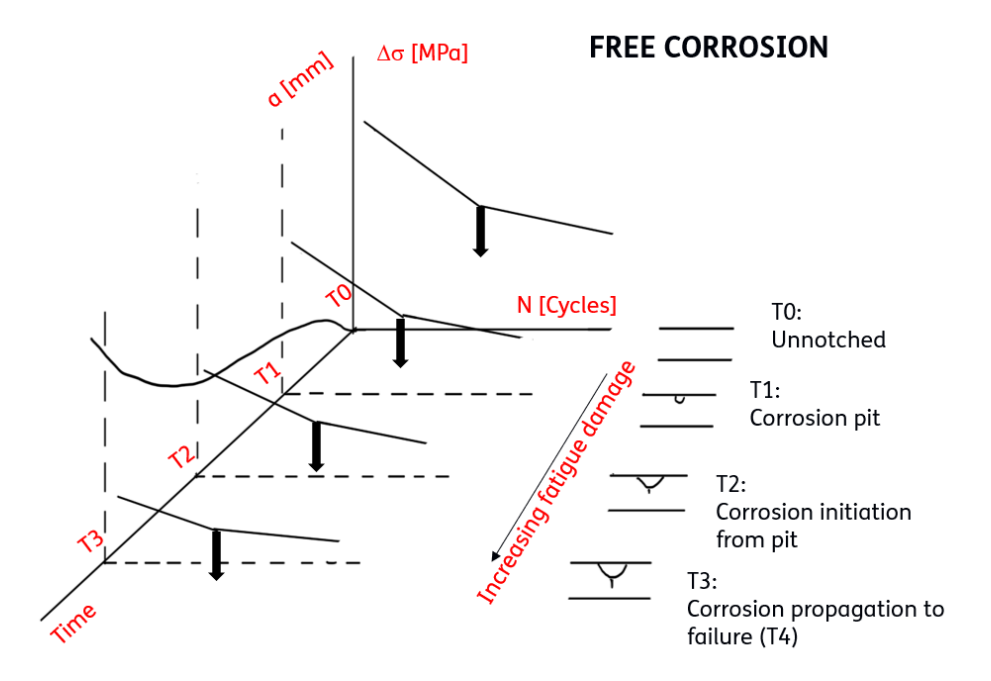


Figure 7.2 - Schematic evolution of S-N curves in zones with free corrosion in time.

The following assumptions are made for the free corrosion environment:

- Localized corrosion is implemented in the corrosion fatigue model by assuming semi-elliptical shaped pits.
- Two corrosion pits are regarded that can coincide and merge into one corrosion pit. The largest stress concentration is when two pits are located edge to edge. The pit nucleation location of the two pits is varied to find the combination that results in the lowest fatigue life.

# 7.4 Modelling results – S-N curves

#### 7.4.1 Fatigue detail categories

In this study three fatigue detail categories have been regarded. According to the DNV standard for fatigue, DNV-RP-C203 [19], these structural (weld) details are:





1. B2-category: base material

D-category: as-welded butt welds
 C1-category: flush ground weld

#### D-category: as-welded butt welds

The D-category is valid for butt welds in plates and flats, or in rolled sections when 100% Magnetic Particle Inspection (MPI) of the weld is performed. The following assumptions are made in the corrosion fatigue model regarding the D-category:

- A weld angle of 30° and a weld toe radius of 1 mm are assumed. Both are conservative estimations based on cross-sections of butt welds as applied in offshore monopiles in the North Sea (provided by Van Oord Offshore Wind [3]).
- The stress ratio R=0.5, because of potential residual stresses due to the welding process, and significant mean stress from load spectra.
- An initial defect size of  $a_i=0.15\,\mathrm{mm}$  is included. The initial defect is modelled as a single corrosion pit.
- Corrosion rate and pit corrosion rate as heat affected zone (HAZ) material (factor 1.6 higher than unwelded steel), see TNO report [11].
- Corrosion pits are located on the weld toe.

#### C1-category: flush ground weld

For flush ground butt welds in rolled plates such as in monopiles, the C1-category may be applied [19]. The following assumptions are made in the corrosion fatigue model regarding the C1-category:

- It is assumed that the weld is completely ground, i.e. no weld angle or weld toe radius are included.
- The stress ratio R=0.5, because of potential residual stresses due to the welding process, and significant mean stress from load spectra.
- An initial defect size of  $a_i=0.15$  mm is included. The initial defect is modelled as a single corrosion pit.
- Corrosion rate and pit corrosion rate as heat affected zone (HAZ) material (factor 1.6 higher than unwelded steel), see TNO report [11].

#### 7.4.2 Atmospheric zone

In the atmospheric zone for scenario 1-3, a coating with a lifetime equal to the design life of the structure is present. A single pit of  $a_i=0.02$  mm is included to mimic the surface roughness for the B2-category, for the C1- and D-category the initial defect of  $a_i=0.15\,$  mm (modelled as single pit) is sufficient and no extra factor for surface roughness is included. It is assumed that at the moment a fatigue crack initiates, the coating cracks and fatigue propagation is in free corrosion conditions. The corrosion rate in the atmospheric zone is 0.15 mm/year. According to DNV-RP-C203 [19], the design curve in air may be used for coating conditions.

#### **D-category**

Figure 7.3 presents the S-N curve from the corrosion fatigue model for the D-category (as-welded butt weld). The graphs shows that the fatigue crack initiation life dominates the total fatigue life up to a stress range of  $\Delta\sigma=50$  MPa. Above this stress range the propagation life is dominating the total fatigue life, and compared to the DNV D-curve in air the S-N curve is more conservative. This is because it is assumed that during the fatigue crack propagation life, a free corrosion environment should be regarded. For stress ranges below  $\Delta\sigma<50$  MPa, the DNV D-curve in air appears to be conservative for this scenario.





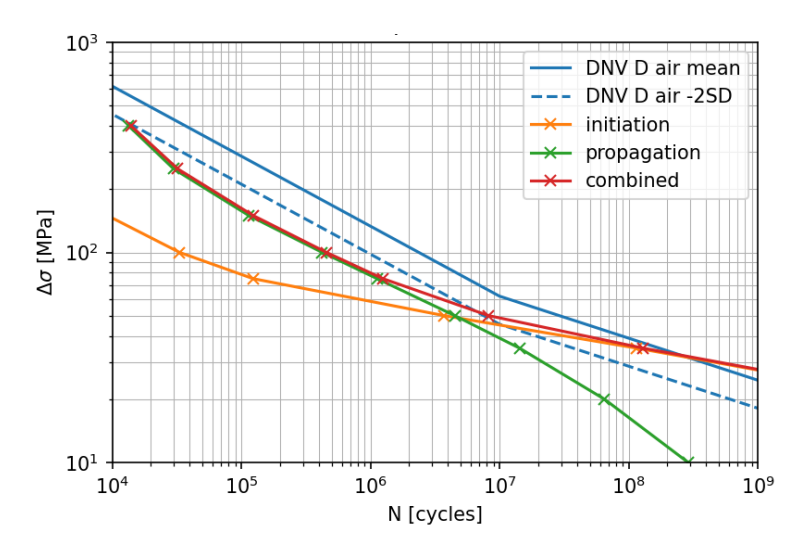


Figure 7.3 - D-category in atmospheric zone with coating. An initial defect (modelled as a single corrosion pit) of  $a_i = 0.15$  mm is included.

## C1-category

Figure 7.4 presents the S-N curve from the corrosion fatigue model for the C1-category (flush ground weld). The result is very comparable to the B2-category. This is expected, because the only difference in the corrosion fatigue model is the starting point of a single pit of  $a_i=0.15$  mm instead of  $a_i=0.02$  mm.

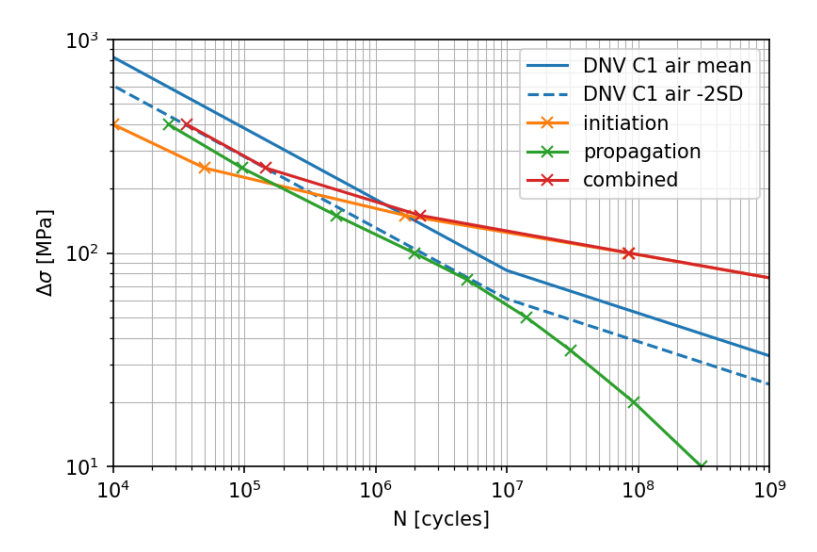


Figure 7.4 - C1-category in atmospheric zone with coating. An initial defect (modelled as a single corrosion pit) of  $a_i = 0.15$  mm is included.

### 7.4.3 Submerged zone

Table 7.1 gives the corrosion mitigation strategies in the submerged zone for scenario 1 to 3 and the accessory starting points for the corrosion fatigue model to distinguish between the scenarios based on coating or ICCP system and period of free corrosion between installation of the monopile and tower (equals start of the considered fatigue load). ICCP is present in all scenarios presented in this section. For all zones and scenarios without coating, interaction between two corrosion pits is included, as indicated in Table 7.1.





Table 7.1 - Corrosion mitigation strategies in submerged zone for scenario 1-3 and accessory starting points in corrosion fatigue model.

		Scenario 1				0	0
		Α	В	С	D	Scenario 2	Scenario 3
Period between installation tower and MP		0 years	0.5 years	1.0 year	1.5 years	1.5 years	1.5 years
Corrosion mitigation		No Coating, GACP / ICCP	No Coating, ICCP	No Coating, ICCP	No Coating, ICCP	Weld coating,	Coating,
Pit size $a_i$	B2-cat.	0.02	0.19	0.59	0.99	0.99	0.02*
	C1/D-cat.	0.17	0.34	0.74	1.14	0.15*	0.15*
Pit interaction		Yes	Yes	Yes	Yes	B2-cat.: Yes C1/D-cat.: No	No

<sup>\* -</sup> A single pit with a pit depth of a = 0.02 mm is included to include surface roughness. For the C1- or D-category, the initial defect size is larger, and therefore considered sufficient.

### D-category: as-welded

Figure 7.5 presents the results of the corrosion fatigue model for scenario 1a to 1d for an as-welded butt welds, compared to the DNV D-category S-N curve in cathodic protection (CP) environment. In the high cycle fatigue region ( $N>10^8$  cycles), the DNV S-N curve appears to be conservative compared to the corrosion fatigue model. For the low and medium cycle domain, the S-N curves are comparable, but depend on the period of free corrosion between installation monopile and CP system. Figure 7.6 presents the total fatigue of scenario 1a to 1d in one graph. The figure shows that a larger initial defect results in a lower fatigue life. When the tower and CP system is installed directly with the monopile (scenario 1a), the S-N curve of the DNV standard is conservative for stress ranges up to 150 MPa compared to the corrosion fatigue model. The other curves intersect at a lower stress range. Figure 7.6 also presents the S-N curve for scenario 2 and 3, i.e. coating and ICCP. The corrosion fatigue model shows a smaller difference between the ICCP environment (scenario 1a to 1d) and coating and CP environment (scenario 3) than the DNV S-N curves for  $N<10^7$  cycles, but a larger difference for  $N>10^7$  cycles. The latter because the DNV S-N curves for air an CP environment are equal for  $N>10^7$  cycles.





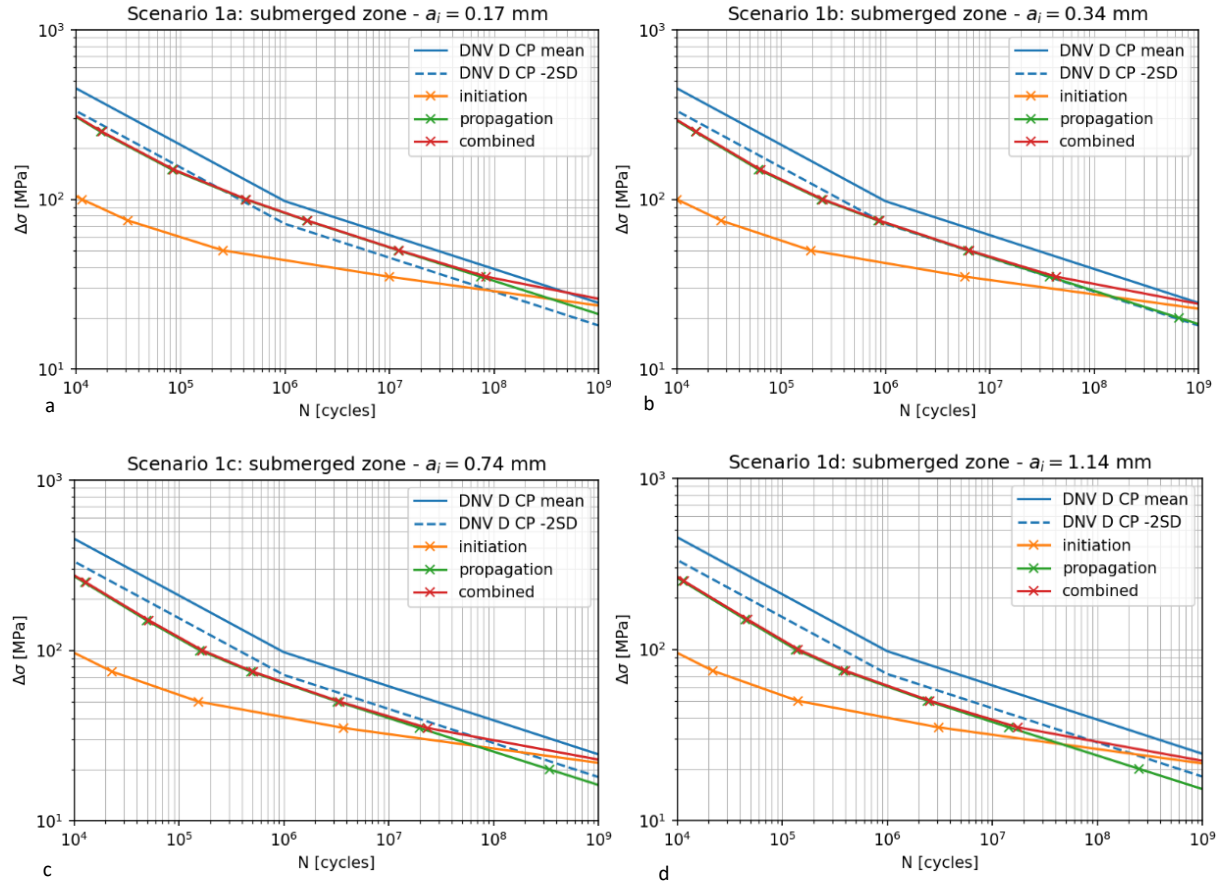


Figure 7.5a to d - As-welded, D-category, in submerged zone for scenario 1a to 1d. Initial pit size  $a_i$  given per graph.

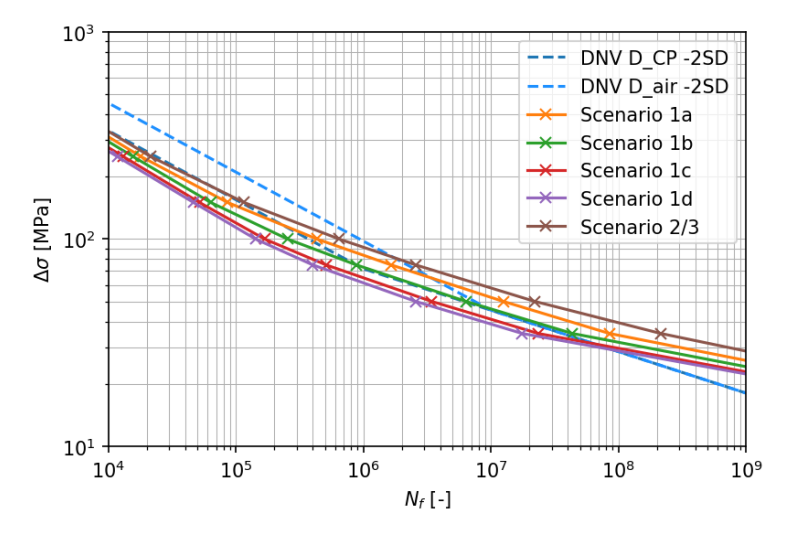


Figure 7.6 - Total fatigue life design curves of D-category in submerged zone for scenario 1-3. Scenario 2 and 3 is with coating, the others without coating.





# C1-category: flush ground weld

Figure 7.7 presents the results of the corrosion fatigue model for scenario 1a to 1d for a flush ground weld, compared to the DNV C1-category S-N curve in cathodic protection environment. Just as for the atmospheric zone, the results are comparable to the B2-category, which is expected because the only difference is the initial defect size of  $a_i=0.15\,\mathrm{mm}$ . Figure 7.8 presents the total fatigue life of scenario 1a to 1d in one graph. The figure shows that a larger initial defect results in a lower fatigue life. When the tower and CP system is installed directly with the monopile (scenario 1a), the S-N curve of the DNV standard is conservative for all stress ranges compared to the corrosion fatigue model. The other curves intersect at a certain stress range. Figure 7.8 also presents the S-N curve for scenario 2 and 3, i.e. coating and ICCP. The corrosion fatigue model shows a larger difference between the ICCP environment (scenario 1a to 1d) and coating and CP environment (scenario 3) than the DNV S-N curves.

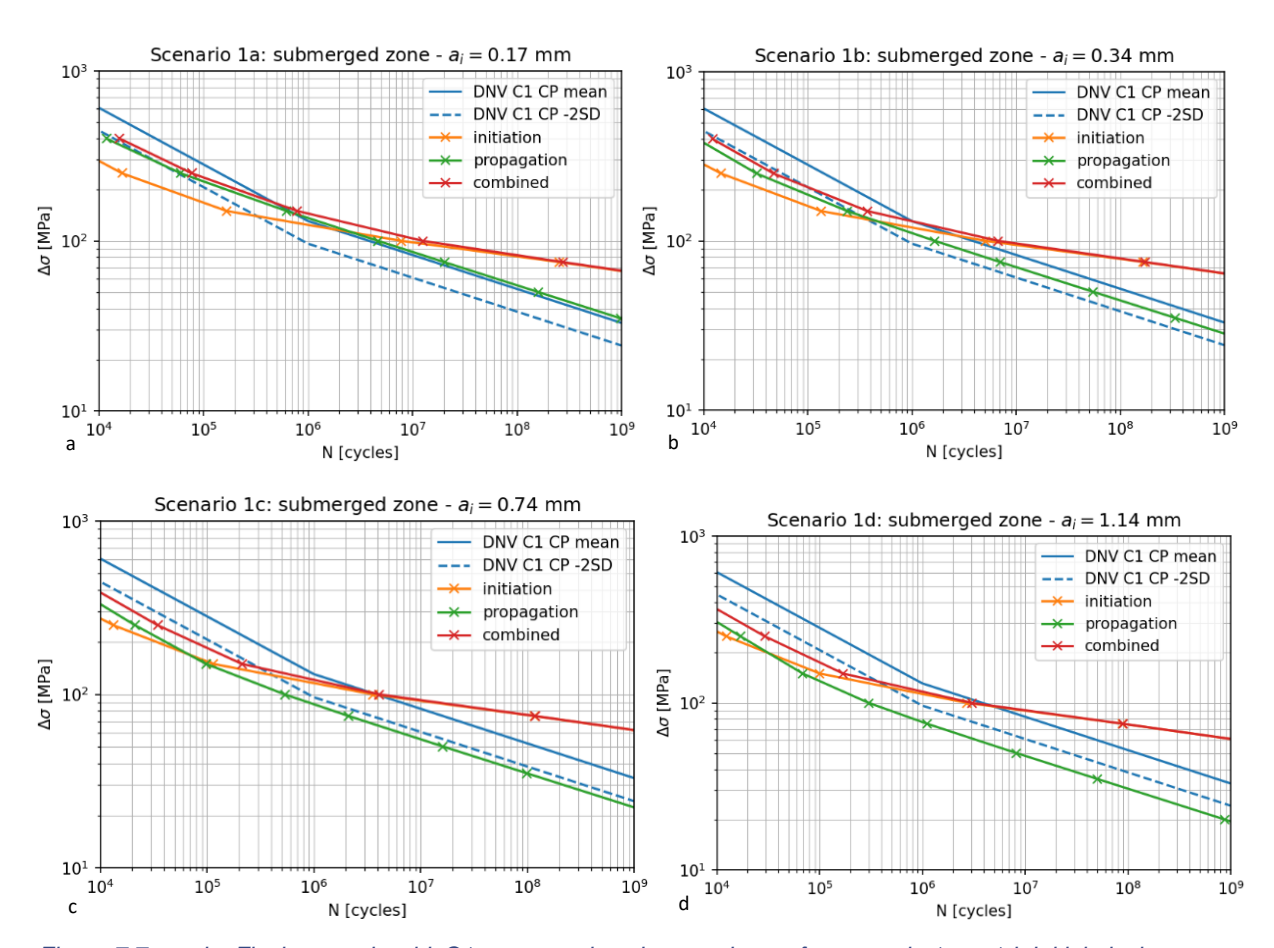


Figure 7.7a to d – Flush ground weld, C1-category, in submerged zone for scenario 1a to 1d. Initial pit size  $a_i$  given per graph.





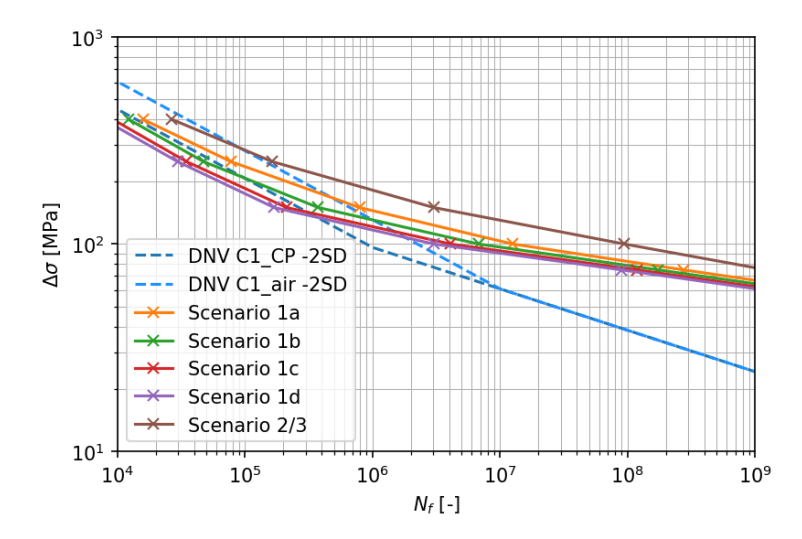


Figure 7.8 - Total fatigue life design curves of C1-category in submerged zone for scenario 1-3. Scenario 2 and 3 is with coating, the others without coating.

# 7.5 Sensitivity analysis

Some results of this sensitivity study are shown for the following input parameters:

- Effect of micro-pit for single pits is considered. For interacting pits, the location between pits gives a larger stress concentration than the (micro-pit) bottom.
- Corrosion pit geometry, the pit aspect ratio ( $AR_p = \alpha/2c$ ) is varied between 0.25 and 0.55. In Rodenburg [22],  $AR_p = 0.40$  has been used.

## 7.5.1 Number of corrosion pits

From corrosion tests and field data, it is found that multiple pits can grow in close vicinity, see TNO/Deltares report [11]. The distance between the edges of the pits, determines whether the location between the pits, or the pit bottom location will result in the location where fatigue crack initiation occurs. Three different configurations of pits are investigated, as presented in Figure 7.9, a single isolated pit, a single isolated pit with a micro-pit in the pit bottom, and two pits in close vicinity. Free corrosion for 7 months between installation of the monopile and activation of the ICCP system in the submerged zone is considered in this section (corrosion protection scenario 1b).

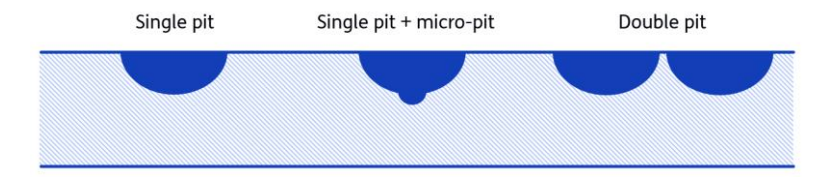


Figure 7.9 - Studied pit configurations

The S-N curves in Figure 7.10 show the results for all three configurations for the construction detail categories according to the DNV standard:

- C1: flush ground butt weld,
- D: as-welded butt weld.

The figure presents the results for the submerged zone, where ICCP is present but no coating. The results present design curves, and should therefore be compared to the design curves of DNV (dashed lines in Figure 7.10).





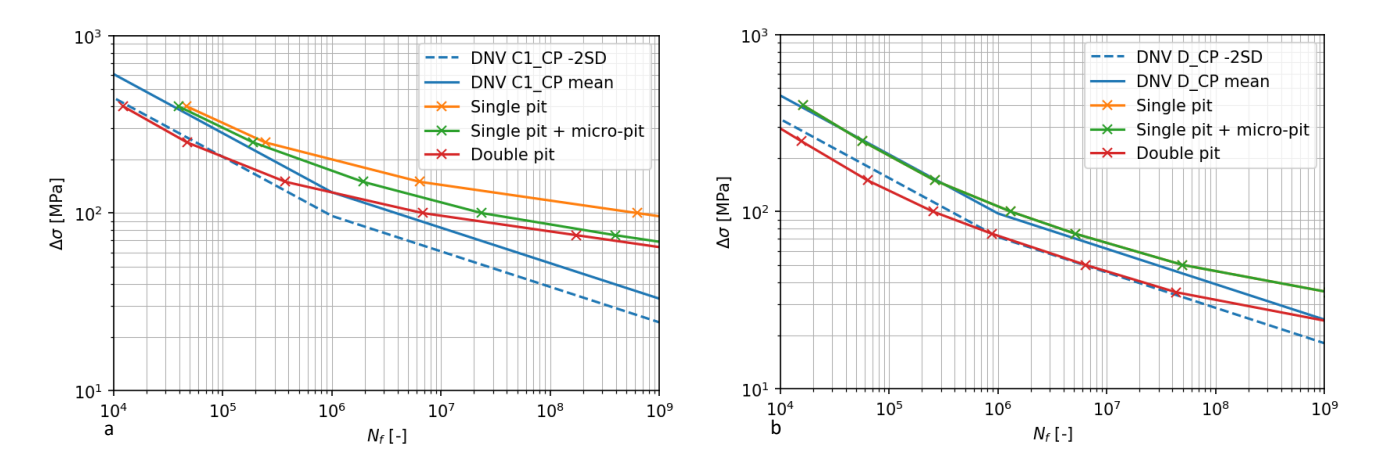


Figure 7.10a/b - Comparison between single and double pit assumption for the submerged zone, where ICCP is present but no coating. Free corrosion for 7 months between installation monopile and activation ICCP system. (a) C1-category, (b) D-category.

Figure 7.10a/b show a significant decrease in the fatigue life of more than a factor 10 when considering double pits instead of single pits for DNV C1-category. For the DNV D-category, this difference is smaller, and the results of single pit or single pit including micro-pit are equal, since the stress concentration of the weld results in initiation at the pit wall (located at the weld toe), instead of in the pit bottom.

# 7.5.2 Corrosion pit aspect ratio

The corrosion pit shape is simplified as semi-elliptical. The aspect ratio  $AR_p$  (width over depth) is determined based on 3D scans of corrosion coupons exposed in the North Sea, and analysed in TNO/Deltares report [11]. In the model, an aspect ratio of  $AR_p = a/2c = 0.4$  is used. This is not the largest aspect ratio encountered in the coupons, but larger than the average of the measured pits. This section studies the effect of a lower and a higher aspect ratio of 0.25 and 0.55 respectively, such as Figure 7.11 shows.

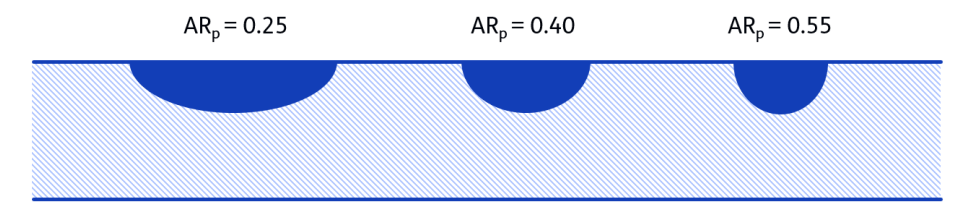


Figure 7.11 - Studied corrosion pit aspect ratios ( $AR_p = a/2c$ ).

Figure 7.12a/b presents the S-N curves from the corrosion fatigue model for the studied aspect ratios for the submerged zone, where the ICCP system is installed 7 months after the monopile, and no coating is present. The S-N curves show that the difference between the aspect ratios is insignificant for the higher stress ranges, where the propagation life is dominating, compared to the lower stress ranges, where the initiation life is dominating.





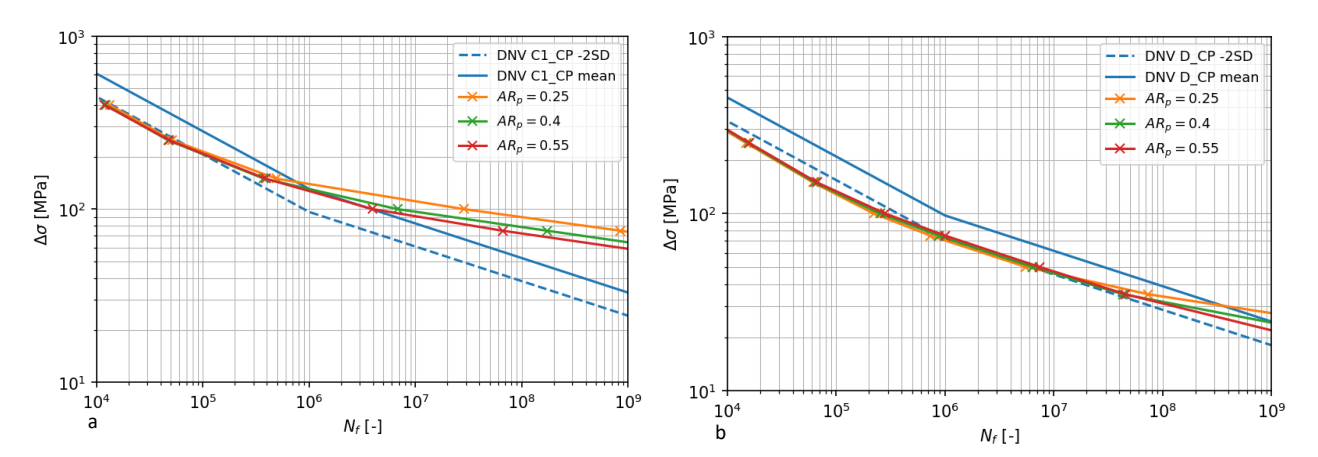


Figure 7.12a/b - Sensitivity on pit aspect ratio  $AR_p$  for the submerged zone, where ICCP is present but no coating. Free corrosion for 7 months between installation monopile and activation ICCP system. (a) C1-category, (b) D-category.

#### 7.6 Conclusions

The C-FLO deterministic corrosion fatigue model has been applied in various corrosion mitigation scenarios regarding the monopile to show the effectiveness of these strategies.

The model can either be used to directly determine the corrosion fatigue life. Alternatively, a procedure has been developed to generate S-N curves for fatigue damage assessment. These S-N curves have been compared with existing S-N curves as presented by the DNV-RP-C203 standard [19] for matching conditions.

The following is concluded based on the comparison of S-N curves according to the C-FLO model (inherently incorporating corrosion fatigue pit growth, crack initiation and crack growth) and the DNV-RP-C203 [19]:

- 1. A larger period between installation of the monopile and installation of the tower (equals installation of the CP system) results in a shorter fatigue life of the monopile.
- 2. For as-welded butt welds, the DNV D-category S-N is conservative for stress ranges in the high cycle fatigue region ( $N < 10^7$  cycles), but unconservative for smaller stress ranges. The latter is due to a difference in assumptions for the propagation life, where for the corrosion fatigue model a propagation curve based on free corrosion conditions is regarded, where the DNV-RP-C203 standard assumes air conditions.
- 3. For flush ground welds, the DNV C1-category S-N curve is conservative for all stress ranges for coating conditions. In particular for lower stress ranges, the C-FLO model predicts longer life, indicating a steeper S-N curve than accounted for by DNV. For cathodic protection conditions, it depends on the period between installation of the monopile and installation of the tower (equals installation of the CP system).
- 4. The difference between the S-N curve for base material and flush ground welds is smaller than according to the DNV-RP-C203 standard.

# 8 Monopile design - WP4

#### 8.1 Introduction

Specific use of the developed corrosion fatigue damage assessment procedure as well as application of the derived S-N curves from the modelling has been focusing on a reference monopile design. The





calculations for the monopile design, have been performed by Van Oord Offshore Wind. Detailed descriptions of the obtained design results can be found in the WP4 report of Van Oord, see Palkar [23], [24]. For the design calculations, reference structural and load data were based on a reference project in the North Sea, for a 9-10 MW wind turbine and a structural design life of 30 years, see Van Oord [2].

## 8.2 Corrosion protection scenarios & Design matrix

The monopile (MP) design calculations have been performed for the selected corrosion protection scenarios presented in Section 2.2 and given in Table 2.2 of this report.

The performed cases of monopile design are:

- I. Redesign of the MP thicknesses considering the design governed by the fatigue limit state (FLS) criterion;
- II. Maintain similar MP design for all the scenarios and compare the total corrosion-fatigue life;
- III. Redesign the MP considering all design criterions, as fatigue limit state (FLS), ultimate limit state (ULS), eigen frequency, and pile diameter to wall thickness (D/t) ratio.

The calculations have been performed for the following subcases:

- a. C-FLO S-N curves as-welded welds
- b. C-FLO S-N curves flush ground welds
- c. DNV S-N curves as-welded welds (D curve)
- d. DNV S-N curves flush ground welds (C1 curve)

A total number of 102 model simulation have been performed for this study.

# 8.3 Case I - Design thickness - Only FLS criterion

In this case study the redesign of the monopile thicknesses in the different zones is governed only by the fatigue limit state (FLS) criterion.

# 8.3.1 As-welded geometry & DNV D-curve

For the as-welded geometry the design wall thicknesses for the different zones as a result of the calculated S-N curves with the C-Flo corrosion-fatigue model, and for these zones based on the S-N curves given by the recommended practice of DNV-RP-C203 (curve D) [19] have been calculated. This has been performed for the corrosion mitigation scenarios given in Table 2.2.

The calculated design monopile wall thicknesses show:

- The S-N curves based on the C-FLO modelling results in the submerged zone, for the free corrosion reference scenario 0, in a thinner design thickness than the ICCP scenarios 1A to 1D. This observation is counterintuitive.
- In all the zones except the splash zone, the C-FLO based S-N curves result in thicker design wall thicknesses than the DNV D-curve. In the splash zone, the resulting thicknesses are comparable.
- In the submerged zone with the C-FLO based S-N curves, the period between the installation of the foundation and the activation of the ICCP, has a significant influence on the design wall thickness.
- The results using C-FLO based S-N curves are very sensitive to the assumption related to the configuration of the corrosion pit double pit vs. single pit.
- Comparing the monopile (MP) weights, in the different zones, over all corrosion mitigation scenarios show:
  - Using the DNV D-curve all the scenarios yield comparable results,





➤ Using C-FLO based S-N curves, the scenarios 2 & 3 with coating strategy yield a lighter design than the scenarios 1A to 1D with an ICCP strategy.

### 8.3.2 Flush ground weld & DNV C1-curve

For the flush ground weld geometry the design wall thicknesses for the different zones as a result of the C-FLO based S-N curves for this geometry, and for these zones based on the DNV C1-curve have been calculated. This has been performed for the corrosion mitigation scenarios given in Table 2.2.

The calculated design monopile wall thicknesses show:

- The designs calculated with C-FLO based S-N curves for a flush ground weld result in thinner wall thicknesses as compared to the designs based on the DNV C1-curve for all scenarios, over all the zones, and for both single and double pit assumptions.
- In the submerged zone using the C-FLO based S-N curves, the period between the installation of the foundation and the activation of the ICCP has a significant influence on the design wall thickness.
- Comparing the MP weights over all the design scenarios;
  - ➤ Using the C-FLO based S-N curve for a flush ground weld, the foundation design for scenario 3 is the lightest followed by scenario 2. The scenarios 2 & 3 with a coating strategy yield lighter designs than the scenarios 1A to 1D with the ICCP strategy.
  - > Overall, the designs based on the C-FLO based S-N curves for flush ground welds are lighter than the designs based on the DNV C1-curve by about 40 %.

#### 8.4 Case II - Design fatigue life - Only FLS criterion

The results for the as-welded geometry and the DNV D-curve, can also be presented as a design fatigue life given a refence wall thickness. The same can be done for flush ground welds and the DNV C1-curve.

The design fatigue life results show:

- For the as-welded geometry that the design fatigue life using the C-FLO based S-N curves are shorter than using the DNV D-curves in nearly all zones (only the splash zone is an exception) and all corrosion mitigation scenarios.
- For flush ground welds, the fatigue life which was close to the design life of 30 years using the DNV C1-curve is almost 5 times when using the C-FLO based S-N curves.
- This enhanced design fatigue life when using the C-FLO based S-N curves for flush ground welds can be realized for lifetime extension of the existing of wind farms.

### 9 Conclusions & Recommendations

#### 9.1 Conclusions

The overall objective of the C-FLO project is to *develop an advanced corrosion pit growth and fatigue crack initiation and growth model for the service life prediction of monopile foundations in the North Sea*.

The model aims at optimising the monopile design and maintenance based on the improved understanding of the combined effect of corrosion and fatigue on the service life of monopile foundations. The optimised design of the monopile and corrosion protection systems leads to a reduced CAPEX in material use and installation, and optimised maintenance strategies brings down the OPEX.





In addition, the model enables quantification of effects on the service life due to the temporary absence of cathodic protection.

# **Corrosion mitigation scenarios**

The study considered four corrosion mitigation scenarios for the different zones of the monopile atmospheric zone, splash & tidal zone, submerged zone, Top 3 m of buried zone and the buried zone. Scenario 0 reflects the base case without application of coating or cathodic protection. Scenarios 1 up to 3 gradually increase the amount of coating and cathodic protection to be applied in the various zones in which also the period between installation of the turbine and the MP is increased.

### **Corrosion fatigue model**

A deterministic corrosion fatigue model is developed to determine the fatigue life of base material and welded components in steel structures incorporating the combined corrosion and fatigue degradation mechanisms. The model is based on various stages of degradation, uniform and local corrosion, transition from corrosion pit to fatigue crack through crack initiation and propagation. The input parameters to the model reflect both geometrical aspects, describing the pit shape evolution as well as the influence of welds resulting in local stress concentrations, as well as typical material parameters, reflecting the resistance to corrosion and fatigue.

In addition to a deterministic corrosion fatigue model, the C-FLO study provides a fundamental approach towards modelling extensive corrosion pit growth modelling and corrosion pit growth in a mechanically loaded steel specimen. The modelling approach is illustrated by two examples: 1) A two-dimensional corrosion pit growth test with mechanical load and 2) a C-ring test.

### **Experimental results**

Three sources have been used: 1) Field data have been studied that focussed on pit corrosion as measured on coupons that were exposed in the vicinity of offshore monopiles; 2) Experiments have been performed to determine pit corrosion rates with and without MIC conditions; 3) Literature data have been analysed.

Corrosion-fatigue crack initiation tests have been performed using specimens containing an artificial corrosion pit in artificial seawater. During these tests extensive electro-chemical measurements using a dedicated potentio-static device have been performed. The corrosion-fatigue crack initiation life has been determined for an estimated life up to a crack size of approximately  $a = 100 \mu m$ 

Corrosion-fatigue tests with large welded specimens on dogbone coupons are executed at Vattenfall. The test results are close to or above the MEAN+2SD line estimates according to DNV RP C203. C-FLO model predictions (MEAN) are close to the experimental data. Base material from Posco shows runouts at a level of 270 MPa (>1.15 million cycles) whereas two of the reference material specimens cracked earlier.

# Model results applied in S-N curves

The C-FLO deterministic corrosion fatigue model has been applied in various corrosion mitigation scenarios regarding the monopile to show the effectiveness of these strategies.

The model has been used to directly determine the corrosion fatigue life, particularly in case of free corrosion. Alternatively, a procedure has been developed to generate S-N curves for fatigue damage





assessment. These S-N curves have been compared with existing S-N curves as presented by the DNV-RP-C203 [14] for matching structural and environmental conditions.

The evaluation of various corrosion mitigation scenarios shows that a larger period between installation of the monopile and installation of the tower (equals installation of the CP system) results in a shorter fatigue life of the monopile. For as-welded butt welds, the DNV D-category S-N is conservative for stress ranges in the high cycle fatigue region (N <  $10^7$  cycles), but unconservative for smaller stress ranges. The latter is due to a difference in assumptions for the propagation life, where for the corrosion fatigue model a propagation curve based on free corrosion conditions is regarded, where the DNV guideline assumes air conditions. For flush ground welds, the DNV C1-category S-N curve is conservative for all stress ranges for coating conditions. For cathodic protection conditions, it depends on the period between installation of the monopile and installation of the tower (equals installation of the CP system). The difference between the S-N curve for base material and flush ground welds is smaller than according to the DNV standard.

# Monopile design evaluation using C-FLO based and DNV based S-N curves

The C-FLO model has been applied to evaluate the following cases of monopile design:

- I. Redesign of the MP thicknesses considering the design governed by the fatigue limit state (FLS) criterion;
- II. Maintain similar MP design for all the scenarios and compare the total corrosion-fatigue life;
- III. Redesign the MP considering all design criterions, as fatigue limit state (FLS), ultimate limit state (ULS), eigen frequency, and pile diameter to wall thickness (D/t) ratio.

The calculations have been performed for the following subcases:

- a. C-FLO S-N curves as-welded welds,
- b. C-FLO S-N curves flush ground welds,
- c. DNV S-N curves as-welded welds (D curve),
- d. DNV S-N curves flush ground welds (C1 curve).

The results in Case I and Case II, where only the fatigue limit state (FLS) criterion was considered, is the upper bound. During foundation design, other design criteria like ULS, D/t ratio, and frequency also play a crucial role.

It is expected that for future foundations with larger turbines and in deeper waters, the designs will become more critical to the fatigue limit state (FLS) criterion. This is of course location specific. For designs that are FLS driven, the impact of different corrosion protection scenarios and C-FLO based S-N curves versus current DNV S-N curves can be expected to be considerable in the design as was observed in Case I and Case II calculations.

The largest difference in design life using the C-FLO model or the DNV RP C203 is found in flush ground welds. For unground welds, there is a large dependency on the assumed influence of either a single (C-FLO less conservative than DNV) or a double corrosion pit (C-FLO more conservative than DNV).





#### 9.2 Recommendations

#### Field data evaluation

- 1. Expose welded samples in free corrosion and cathodic protection environment in the vicinity of monopile location with a minimal exposure time of two to four years preferably under realistic stress conditions.
- 2. Get more clarity on the likelihood of double pits versus single pits in base material and welds.
- 3. Assess the influence of stress level on pit growth, to be validated in the field for free corrosion and cathodic protection after free corrosion.
- 4. Investigate distribution and shape of pits in unground welds. Assess the notch stress.
- 5. Assess samples from decommissioned wind farms for evaluation shape and number of pits, preferably with long exposure periods.

# **MIC** testing

- 1. Assess the effectiveness of CP against MIC
- 2. Assess effects of nutrients on MIC and relate these to field conditions
- 3. Assess how often MIC occurs in the field

### **Corrosion fatigue testing**

- 1. Further validate the outcome of the corrosion fatigue model to corrosion fatigue tests in air, seawater and seawater with cathodic protection environment.
- 2. Increase data pool for validation of models, especially focus on low stress ranges and initiation
- 3. Apply simultaneous CP, microbial activity and fatigue
- 4. Use specimens from the field with realistic pit size.
- 5. Increase data pool for crack growth rate in corrosive environment for cases with welded connections and cathodic protection.
- 6. Further test with OCP method for tracking crack initiation in specimens with realistic pit.

#### Improve model

- 1. Increase reliability of the predicted S-N curves supported by validation tests.
- Assess uncertainties of input variables to the model and perform full probabilistic evaluation of these influence parameters towards increasing robustness of the model and improving the reliability of the model output.
- 3. Perform more research in the pit-to-crack transition in combination with short fatigue crack growth.
- 4. Improve the link between the fundamental model (TU Delft) and the corrosion fatigue model (TNO).

#### Design and production choices on fatigue

- 1. Assess effect of post weld treatment on corrosion fatigue.
- 2. Make S-N curves independent on wall thickness, misalignment, thickness transition etc.
- 3. Apply C-FLO model for existing structures in case of life extension, updating inspection intervals and/or in case of coating defects.





# 10 References

- [1] Grow Project Proposal, Corrosion Fatigue Life Optimisation (C-FLO), Project number: 201702 03 04 TNO C FLO, June 2019.
- [2] Luiken R., Kourtis I., "Technical Note: C-Flo VOOW input," 9182007-VOOW-TF-ENG-TN-1000, 2022.
- [3] Drawing monopile, "Monopile DWG belonging to loadsets.pdf", Van Oord Offshore Wind, 16-08-2021.
- [4] Norsok M501, Surface preparation and protective coating, 2020.
- [5] DNV-RP-0416, Recommended Practice, Corrosion protection for wind turbines, 2016, Amended October 2021.
- [6] Larrosa N.O., Akid R., Ainsworth R.A., Corrosion-fatigue: a review of damage tolerance models, International Materials Reviews 63(5), 2018, 283-308.
- [7] Lomholt T.N., Mathiesen T., Egelund S., Bangsgaard D.B., Unification of monopile corrosion protection collaboration in partnerships, 51318-11170-SG, NACE Conference 2018.
- [8] Rodenburg J.D., Predicting the Pit-to-Crack Transition of Offshore Wind Turbine Foundations A mechanistic determination, MSc-thesis, TNO & Delft University of Technology, http://repository.tudelft.nl/, 2020.
- [9] Slot H.M., Rodenburg J.D., Luyten J., Corrosion-fatigue crack initiation Model development, C-FLO project WP2, TNO report, nr: TNO-2023-R10104, 2023.
- [10] Jansen S., Gerritse J., Croese E., Microbiologically Influenced Corrosion (MIC) of steel in seawater in relation to fatigue; Results of laboratory experiments project C-FLO, Deltares report, report nr: 11204675, 2023.
- [11] Rodenburg J.D., Jansen S., Slot H.M., Schuring E.W., Pit corrosion examinations in C-FLO WP3 Quantification of the pit growth rate and pit shape in different seawater environments, TNO report/ Deltares report, report nr: TNO-2023-R10144, 2023.
- [12] Slot H.M., Jansen S., Schuring E.W., Ochôa P., Pijpers R., Corrosion fatigue & Stress corrosion cracking tests in different seawater environments, C-FLO project WP3, TNO report/ Deltares report, report nr: TNO-2023-R10888, 2023.
- [13] Jamar G.T.J., Corrosion-fatigue crack initiation life measurements in artificial seawater, MSc thesis, Delft University of Technology & TNO, 2023.
- [14] Dillinger France, Materials certificate of steel grade S355ML (plate thickness of 15 mm, Certificate no. 447027-002, date of dispatch: 13.06.2019.
- [15] POSCO, Steel with Surface Fine Grain (SFG) Process, Presentation, Steel Structure Research Group of POSCO, 7 October 2019.
- [16] Adedipe O., Brennan F., Mehmanparast A., Kolios A., Tavares I., Corrosion fatigue crack growth mechanisms in offshore monopile steel weldments, Fatigue & Fracture of Engineering Materials & Structures 40, 2017, 1868-1881.
- [17] Fayezioghani A., Dekker R., Sluys L.J., Verification, validation, and parameter study of a computational model for corrosion pit growth adopting the level-set method. Part I: Corrosion, Materials Today Communications 33 (2022) 104525.
- [18] Fayezioghani A., Dekker R., Sluys L.J., Verification, validation, and parameter study of a computational model for corrosion pit growth adopting the level-set method. Part II: Stress corrosion, Materials Today Communications 33 (2022) 104210.
- [19] DNV-RP-C203, Fatigue design of offshore steel structures, Recommended Practice, Edition 2019-09 - Amended 2021-09, Det Norke Veritas AS, 2021.
- [20] DNV-OS-C401, Fabrication and Testing of Offshore Structures, Det Norke Veritas AS, 2020.
- [21] Rodenburg J.D. Corrosion fatigue modelling results Report on S-N curves, C-FLO project WP4, TNO report, report nr: TNO-2023-R10889, 2023.







- [22] Rodenburg J.D. Corrosion fatigue modelling Sensitivity analysis, C-FLO project WP4, TNO report, report nr: TNO-2023-R10890, 2023.
- [23] Palkar S.S., WP4 Monopile design calculation using C-FLO curves, Presentation Van Oord, 29 April 2023.
- [24] Palkar S.S., Design Report: Fatigue design of Monopile using C-FLO curves, Document Number: 9182007-VOOW-TF-ENG-REP-1001, Van Oord Offshore Wind B.V., 2023